Check for updates

Chiral plasmonic nanostructures: recent advances in their synthesis and applications

Wenbing Wu and Matthias Pauly [ID] *

Chirality describes the geometric property of an object that is not superimposable on its mirror image and has been a pivotal concept in chemistry and biology since the 19th century. Chiral plasmonics has attracted increasing attention over the past years as modern nanofabrication techniques and soft-chemistry synthesis and assembly approaches have allowed the preparation of complex and well-controlled chiral metallic nanostructures with promising applications in fields such as molecular sensing and chiral separation and synthesis, or as optical polarizing elements. This review covers the main techniques employed to construct chiral plasmonic materials, in particular using soft-chemistry approaches, and discusses some applications of these nanostructures on the basis of recent examples drawn from the literature.
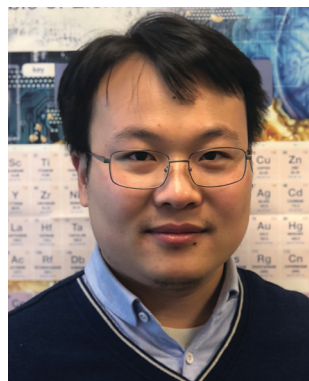
1. Introduction

Chirality is the geometrical property of an object lacking any planes of symmetry or inversion centers which distinguishes the original object from its non-superimposable mirror image – a chiral object and its mirror image are called enantiomorphs, or when referring to molecules, enantiomers.[1] Human hands are the most explicit illustration of this concept, and the word

Université de Strasbourg, CNRS, Institut Charles Sadron UPR22, 67000 Strasbourg, France. E-mail: matthias.pauly@unistra.fr

"chirality" is derived from the word "hand" ($\chi \in \iota \rho$ or kheir) in ancient Greek.

It was Lord Kelvin who coined the term in 1893:[2] "I call any geometrical figure, or group of points, 'chiral', and say that it has chirality if its image in a plane mirror, ideally realized, cannot be brought to coincide with itself", although the concept of molecular chirality had already been discovered by Louis Pasteur in 1848, while investigating the enantiomers of a tartaric acid salt,[3,4] and described as "dissymmetry" at the time. It was not until 25 years later that Le Bel[5] and van't Hoff[6] established the basis of molecular stereochemistry by formulating the notion of asymmetrical tetrahedral carbon atoms.

Wenbing Wu obtained his PhD from the University of Strasbourg (France) under the guidance of Prof. Gero Decher in 2020. He is now a postdoc research fellow in Prof. Nicholas A. Kotov's group in the Department of Chemical Engineering, University of Michigan in Ann Arbor (USA). His current research interests include layer-by-layer assembly, chiral plasmonic nanostructures, self-assembly of inorganic nanoparticles and nanocomposite metamaterials.

Wenbing Wu

Matthias Pauly is an assistant professor at the chemistry faculty of the University of Strasbourg (France). He obtained his PhD on the assembly of magnetic nanoparticles in 2010 at the Institute of Physics and Chemistry of Materials (IPCMS) in Strasbourg before joining the Nanoscale Science Department of the Max Planck Institute for Solid State Research in Stuttgart (Germany) as a postdoctoral fellow working on Electrospray Ion Beam Deposition. Since 2012 he works at the Institut Charles Sadron (CNRS, University of Strasbourg) on the assembly of anisotropic nanoparticles into complex superstructures and the characterization of their optical and electronic transport properties.

Matthias Pauly

Since then, the concept of chirality has been steadily expanding as a major topic in chemistry and biology, owing to its wide occurrence and paramount importance in nature and the related potential applications. The fact that, for instance, homochirality[7] is favored in living systems on earth is thought to be a possible origin of life.[8,9] Indeed, all amino acids (with the exception of glycine), which constitute the essential components of proteins and enzymes, are levogyre, whereas the sugars that are the essential components of DNA and RNA are all dextrogyre. Nowadays, more than 50% of the drugs currently in use are chiral, most of which are marketed as a racemic mixture.[10] In certain cases, only one enantiomer is a drug while the other one is a poison. One tragic example is thalidomide, a drug given in the 1960s to pregnant women to treat morning sickness, which caused the delivery of over 10 000 children with severe birth defects, such as phocomelia. Several years later, it was proven that the clinically active component was (R)-thalidomide, while (S)-thalidomide was extremely teratogenic, although its pathological mechanism was not elucidated until 2010.[11] Many other examples showing the importance of chirality in biology can be cited, such as the chiral fragrance of molecules[12,13] in fruits producing different odors. For instance, R-(+)-limonene has an orange scent while L-(−)-limonene has a turpentine-like odor.[14,15] Similarly, R-(−)-carvone, or L-carvone, has a minty smell while S-(+)-carvone has a spicy aroma like caraway seeds.[16]

Chirality is not limited to molecular systems but may appear on all scales, ranging from spiral galaxies[17] to nanoscale structures.[18] Accompanying the development of nano-sciences and technologies, the fabrication and investigation of artificial chiral nanostructures, from the molecular level[19] and supramolecular (self-)assemblies[20–23] to chiral (multimaterial) nano- and microstructures, have been the subject of intense research, owing to the many potential applications in biology, pharmacy, chiral catalysis, light manipulation and light–matter interaction.

Beyond its purely geometrical description, chirality also manifests itself through specific optical properties. Indeed, different enantiomers have different complex refractive indices for right- and left-handed circularly polarized (RCP and LCP) light, which can be described as "chiral light". The difference in the imaginary part of the refractive index results in circular dichroism (CD), i.e., a different absorption of RCP and LCP light, while the difference in the real part leads to circular birefringence (CB), which causes the rotation of a linearly polarized light field from its original orientation while traveling through a chiral medium. The upper scale where chirality emerges and chiroptical phenomena can be detected is of the order of the wavelength of the light used to probe the optical activity. The chiroptical properties of (bio)molecules, which arise on the molecular scale, manifest themselves in the UV-visible range and this mismatch makes the optical activity inherently weak. Surface plasmon resonances, which arise due to the coherent collective excitation of free electrons at the interface between two materials with opposite permittivities (typically a metal and a dielectric), result in the confinement of light on the nanoscale and have thus been used to boost various optical phenomena including chiroptical effects.[24,25]

Small metallic particles lead to the non-propagating confinement of light and to localized surface plasmon resonances, which create strong electric and magnetic dipoles located on the nanoparticles. A chiral particle (or a chiral assembly of interacting non-chiral particles) can be described as a coupled system of induced electric and magnetic dipole moments which interact differently with LCP and RCP light. Indeed, the shape of the particle/assembly dictates whether a plasmon mode can be excited more efficiently by one circular polarization state as compared to the other one. The large magnitude of those dipoles in plasmonic systems lead to chiroptical signals that are much stronger than those found in molecules.

In this review, we will focus on the fabrication and applications of plasmonic chiral <systems. We will first briefly present some examples of the top-down methods used to build chiral plasmonic nano-objects, before discussing the bottom-up approaches in more detail. We will in particular introduce recent examples of the synthesis of chiral nanoparticles and the different routes explored to build chiral assemblies of non-chiral nanoparticles. In the last section, various applications of such nanostructures will be discussed on the basis of recent examples drawn from the literature.

2. Top-down methods

The top-down approach[26] involves the local elimination of material from a larger object or film in order to obtain the desired shape, layout and properties, using technologies such as direct laser writing (DLW), focused ion beam etching, and optical or electron-beam lithography. The gammadion is an archetypal "planar" chiral shape that has been widely studied.[27–33] The optical chirality in such a planar structure arises not only from its "2D chiral" shape (any 2D structure is intrinsically mirror-symmetric and thus inherently achiral in 3D space), but also from the difference between the air–sample and sample–substrate interfaces that is required to break the symmetry.[28] On the contrary, the helix shape is a typical chiral structure and the top-down fabrication of metallic helices, especially gold and silver, has been extensively studied.[34–37] For example, J. K. Gansel et al.[38] obtained gold helix arrays by DLW, which display a different transmittance for LCP and RCP light in the mid-infrared regime (Fig. 1A). In a positive photoresist, two-photon direct laser writing was used to produce helical pores, which were then filled with gold by electrochemical deposition. A free-standing array of gold helices was thus obtained by eliminating the residual polymer mold by plasma etching. This work largely extended the spectral width of plasmonic chiroptical effects and exhibited potential for controlling these effects by tuning the structural parameters including the pitch and diameter of the helices.[39] More complex metallic helical nanostructures were reported several years later by A. Radke et al. (Fig. 1B).[40] These authors combined DLW with electroless silver plating, an autocatalytic process allowing the deposition of silver in the helical voids

Fig. 1 (A) (a) Oblique view of an array of left-handed gold helices. (b) Experimental and modeled transmittance spectra of right-handed helices for LCP (blue lines) and RCP (red lines) light.[38] Copyright 2009 American Association for the Advancement of Science. (B) (a) The four possible combinations of chiral helices and corners.[41] Copyright 2009 John Wiley and Sons. (b) Oblique view of a bichiral crystal with right-handed corners and helices. (c) and (d) Transmittance spectra of a bichiral crystal with left-handed corners and helices (c) and right-handed corners and helices (d) for LCP (black lines) and RCP (red lines) light at an incident angle of 0° (left spectra), and the corresponding difference in transmittance (right spectra).[40] Copyright 2011 John Wiley and Sons. (C) SEM images of (a) a left-handed etch pit formed by anisotropic etching of [137] Si, (b) the same pit with a 50 nm deposit of Au and (c) the left-handed Au nanopyramid extracted from the pit. Experimental CD spectra of left- and right-handed chiral Au nanopyramids deposited (d) with the wafer tilted and rotated during deposition and (e) with the wafer normal to the incident flux. (f) SEM image of left-handed gold nanoparticles.[45] Copyright 2014 American Chemical Society.

previously obtained by DLW. Both left- and right-handed helices were constructed ("chiral helices"). The helices were arranged in a cubic lattice with their axes ordered in both left- and right-handed fashions ("chiral corners"). The structures obtained were therefore referred to as bichiral[41] crystals, which

have four possible combinations stemming from their two levels of chirality. The chiroptical effects were found to be enhanced for combinations of helices and corners with the same handedness and reduced for those with different handedness. Meanwhile, metallic crystals have shown much

stronger chiroptical activities in the MIR range as compared to their dielectric counterparts[41] due to plasmonic resonance. Spiral-type ramp nanostructures with chiroptical properties in the NIR range were obtained by B. Frank et al.[42] using so-called "colloidal nanohole lithography".[43,44] These structures displayed bisignate differential transmittance (ΔT) for LCP and RCP light, with symmetrical chiroptical properties for left- and right-handed enantiomorphic forms. The maxima and minima of ΔT were found to lie at the plasmonic resonance positions, and the interaction between circularly polarized light and the chiral nanostructure could be successfully explained by a dipole model developed by the authors.

Other chiral structures besides helices can also be obtained using top-down approaches. For example, chiral surface structures and gold colloids have been produced by the controlled etching of high-index silicon wafers (Fig. 1C).[45] This very original process is based on the slow etching of the [111] atomic planes of silicon wafers in potassium hydroxide. By etching [137]-oriented wafers through holes with a specific shape in a silicon nitride mask, a chiral pit with smooth facets is obtained, which can be used as a template onto which gold can be evaporated, leading to large-area chiral surfaces. Interestingly, selective removal of the metallic film from the pits may be employed to produce chiral gold nanoparticles exhibiting circular dichroism in the visible range.

Many other examples may be cited where lithography has been used as a top-down fabrication method. Dietrich et al. built an array of chiral nanostructures by on-edge electron beam lithography (Fig. 2A).[46] An electron-beam resist film was spin-coated onto a pre-structured surface and L-shaped gold nanoparticles were deposited by e-beam lithography on the edge of the corrugated striped pattern, leading to a chiral material displaying strong circular dichroism in the NIR range. More recently, the use of DNA origami structures as a lithography mask to produce chiral plasmonic nanostructures was reported (Fig. 2B).[47] The advantages of using DNA origamis as the mask as compared to conventional lithography techniques are their structural versatility and high productivity, which permit more effective nanofabrication over a large area. Chen et al. recently demonstrated that an on-chip and electromechanically reconfigurable nano-kirigami could be constructed on an Au/SiO$_2$/Si substrate by e-beam lithography.[48] Broadband non-resonant and narrowband resonant optical reconfigurations were achieved at visible and near-infrared wavelengths. In another report, Guan et al. used colloidal lithography to prepare arrays of so-called "hollow nanovolcanos", which could be transferred to flexible substrates or hydrogels, thus enabling the ultrasensitive detection of the water content in the gels.[49]

Top-down approaches are suitable for the fabrication of nanoparticles or nanocrystals with a chiral geometry as any shape can be designed at will (the only limit being the size of the structure). However, most studies have focused on assemblies of similar nano-objects placed in a 2D plane either at random positions or ordered on a regular 2D array.[24,50]

On the other hand, chirality can also arise from the multilayer stacking of non-chiral nano-objects twisted at an angle with respect to each other.[51–60] It is nevertheless much more difficult to prepare complex chiral assemblies with a hierarchical arrangement of the building blocks using top-down approaches.[61] One representative example of such materials is the twisted multilayer structure composed of aligned gold nanorods developed by Y. Zhao et al. (Fig. 2C).[54] A single layer of aligned gold nanorods was deposited using e-beam lithography similarly as in the other procedures described above, before depositing a dielectric spacer layer. The process was then repeated to produce multilayer structures with a twist angle between adjacent layers. Strong differential transmission for LCP and RCP light stemming from the interlayer plasmonic coupling was measured in the visible range, and the chiroptical effects were shown to be dependent on the number of stacks in the multilayer structure. Another form of twisted multilayered structure has been proposed by Wu and Zheng: two identical gold nanohole arrays were prepared by colloidal lithography using polystyrene particles as lithographic masks and stacked at a small angle into a moiré pattern.[51] The same group later demonstrated that such a moiré pattern can be actively tuned using thin films of silk fibroin protein as spacers.[62] The silk fibroin undergoes highly controllable swelling in response to the polarity of surrounding solvents, allowing to tune the spacing between the two nanohole arrays.

While well-defined nanostructures can be produced by lithographic techniques (and more generally top-down approaches), they often require multistep processes and expensive vacuum-based equipment. In particular, the building blocks need to have subwavelength dimensions, i.e., of the order of tens of nanometers for applications in the visible and UV range, which is challenging, even for e-beam lithography. Obtaining well-defined nanostructures over large areas is also difficult, although some top-down approaches like colloidal lithography can face up to this challenge.[25] The problem is even greater in the case of "3D" multilayer nanostructures which require precise alignment of the individual building blocks in each layer. These technologies are also inherently restricted to small areas, which limits our capacity to produce macroscopic-scale materials.[63] Bottom-up techniques have thus been proposed in recent years as an alternative approach to address these issues.

3. Bottom-up methods

As opposed to top-down methods, the bottom-up approach[26,63–65] involves arranging small particles into more sophisticated hierarchical structures and assemblies, in which the material properties attained go beyond the sum of the properties of the individual building blocks. Chiral plasmonic nanostructures can be synthesized using various techniques, the chirality being obtained either through chiral arrangement of the particles by controlling the external constraints during
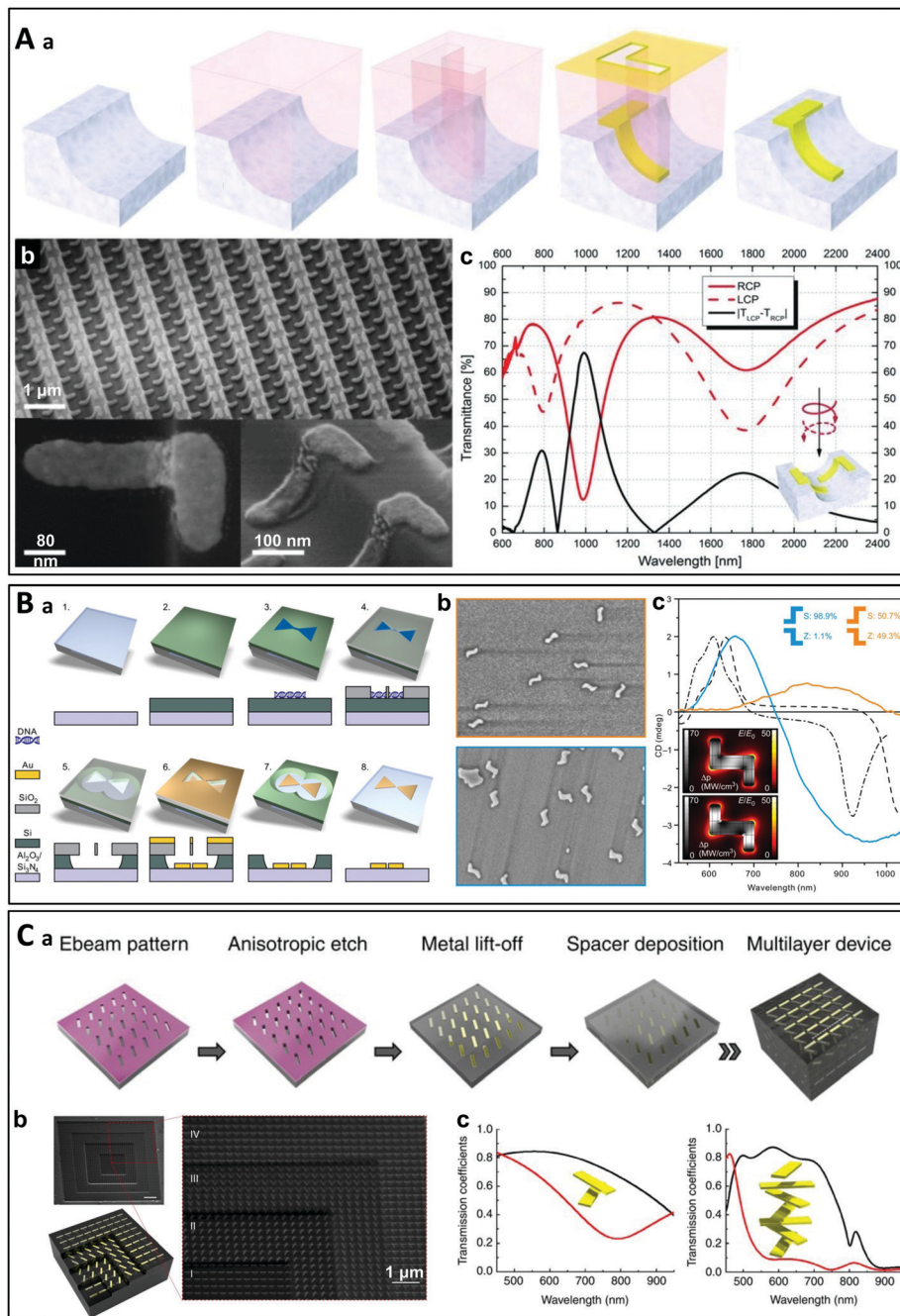
Fig. 2 (A) (a) Schematic representation of the on-edge lithography method, where L-shaped gold particles are deposited by e-beam lithography on the edge of the stripes of a pre-patterned substrate. (b) SEM images of the resultant chiral nanomaterial array. (c) Simulated transmittance spectra of a 3D L-particle array for RCP and LCP light and their intensity difference.[46] Copyright 2012 John Wiley and Sons. (B) (a) Schematic representation of the lithography process in which DNA origami nanostructures are used as a mask (the bow-tie shape shown here is non-chiral). (b) SEM images of samples containing a 50:50% (racemic) distribution of S- and Z-shaped nanostructures (top) and ~99% S-shaped nanostructures (bottom). (c) Measured CD spectra of the samples shown in (b) and simulated CD responses for symmetric (dashed) and slightly asymmetric (dash-dotted) S-shaped chiral nanoparticles.[47] Reproduced under the terms and conditions of the CC-BY license. (C) (a) Schematic representation of the lithographic fabrication of a multilayered chiral nanostructure. (b) SEM images of a four-layer device using samples prepared by focused ion beam milling to reveal each layer. (c) Transmittance spectra of a two-layer and a four-layer device for LCP and RCP light.[54] Copyright 2012 Springer Nature.

assembly (for instance using shear forces that induce a linear anisotropy to build oriented layers of 1D nanoobjects that can be stacked into a Bouligand structure) or by means of chiral templates. As compared to top-down methods, bottom-up approaches are often faster, less expensive and more adaptable to prepare arbitrary structural geometries over a larger range of scales.[66]

3.1. Chiral architectures obtained by vacuum-based bottom-up approaches

Many bottom-up techniques using vacuum-based deposition of a metal precursor or metal vapor have been employed to fabricate chiral nanostructures of various shapes, including helices.[67] Thus, focused ion beam and electron beam induced deposition (FIBID/FEBID) are two classical examples of bottom-up methods.[68–70] They consist of depositing materials contained in a vaporized precursor molecule which is decomposed by an ion/electron beam (Fig. 3A). The gases are delivered to the substrate through an injection nozzle located close to the surface. The precursors are decomposed by the focused ion/electron beam, leading to local deposition of the materials on the substrate. Nanostructures with a specific shape and pattern can be obtained using gas injection systems with multiple channels and/or by changing the experimental conditions. For example, archetypal chiral nanohelices may be synthesized using these techniques. M. Esposito et al. prepared chiral platinum nanohelices which exhibited chiroptical effects in the visible range, employing and comparing FIBID and FEBID (Fig. 3A).[71] These authors demonstrated their nanoscale control over the geometrical features of the structures, which allowed them to obtain tunable chiroptical effects in the optical frequency range. However, as such helices are "written" one by one by the focused electron/ion beam, only a limited number of nano-objects can be produced in a reasonable time (arrays of up to 40 × 40 nanohelices were synthesized in this study).

Another related approach to fabricate chiral (helical) nanostructures is known as glancing angle deposition (GLAD, Fig. 3B).[72–80] The idea is to deposit and grow materials on seeds (e.g., Au nanodots) pre-located on the substrate by vapor deposition at a grazing angle and/or by rotating the substrate. The helices are formed through shadowing effects. This technique allows the efficient synthesis of nanohelices on large surfaces. Vacuum evaporation may also be used to produce chiral nanostructures other than helices. Whereas GLAD can be employed to fabricate chiral helices by rotating the substrate during deposition, a simplified two-step GLAD procedure with a tilt angle leads to simplified chiral shells. Thus, Y. Hou et al. prepared chiral stacked-patch plasmonic metamaterials using two-step GLAD on microspheres (Fig. 3C).[81] B. Yeom et al. synthesized chiral gold shells by depositing gold on ZnO nanopillars at a 45° tilt angle (Fig. 3D).[82] By rotating the sample during deposition of the second layer in a direction different from that of the first layer, left- and right-handed chiral plasmonic nanostructures were obtained. These asymmetric gold nanoshells, although simple, exhibited strong chiroptical effects in the visible range.

3.2. Chiral nanostructures obtained by wet chemistry

3.2.1. Nanoparticles with a chiral shape.
The most obvious approach to obtaining chiral plasmonic nanostructures is to induce chirality at the level of the nanoparticle itself.[83–85] In most cases, a chiral molecule or biomolecule, such as an amino-acid, is used as a template to induce the chiral shape during nanoparticle synthesis.[86] For example, H. Lee et al. employed amino-acids and peptides to guide the growth of chiral gold helicoids on a cubic or octahedral seed (Fig. 4A).[87] The chiral morphology of such nanoparticles results from the different growth rates of the two oppositely chiral high-index gold planes in the presence of chiral biomolecules. By selecting the growth-directing agent (amino-acid vs. peptide) and/or changing the shape of the seed (cubic vs. octahedral), the authors obtained chiral helicoids with different morphologies (Fig. 4A(a–c)). All these chiral helicoids had 432 point group symmetry, and the synthesis was later optimized to produce more homogeneous nanoparticles with an improved g-factor of 0.3.[88] Using one of the helicoids (432 helicoid III, Fig. 4A(c), with a pinwheel shape), A. Miandashti et al. investigated the polarization-dependent photothermal properties of these structures.[89] They found that when exposed to circularly polarized laser excitation at a given wavelength, the temperature of a chiral helicoid nanoparticle (growth-directed with L-glutathione) was higher under right- than under left-polarized irradiation (Fig. 4B). The photothermal heating of the nanoparticles was due to their polarization-dependent absorption cross section and surface plasmon resonance and could be used to characterize the chirality at the single-particle level. Starting from chiral helicoid gold nanoparticles, K. Nam's group has further developed similar structures with a rhombic dodecahedral morphology using cysteine[90] and a cube shape with protruding chiral wings using dipeptides (γ-glutamylcysteine and cysteinylglycine).[91]

Another recent example of the directed growth of chiral nanoparticles was reported by G. González-Rubio et al. (Fig. 5A).[92] Using achiral nanorods as seeds, chiral cosurfactants were adsorbed on the surface of the rods and directed the seeded growth to produce chiral nanorods with helical wrinkles on their surface. These structures displayed very strong chirality (with g-factors of up to 0.2), depending on the dimensions of the nanorods.

An original approach was recently employed by S. Golze et al. to grow helical gold spirals in a light-driven solution-based synthesis (Fig. 5B).[93] In this system, LSPR-generated hot electrons drive the reduction of Au^{3+} on seeds. The rupture of symmetry during growth which leads to chiral spiral structures is a consequence of three factors, the planar defects along the seeds, the capping agent that severely inhibits early-stage growth and the Coulombic repulsion occurring when identically charged growth fronts collide. While the individual particles are chiral, left- and right-handed structures are synthesized in equal numbers (racemic mixture) in the absence of a chirality-directing agent.

3.2.2. Coupling of chiral molecules with non-chiral plasmonic particles.
Chiroptical activity can be induced in the plasmonic band of non-chiral metallic nanoparticles by placing chiral molecules close to their surface.[94–100] The chirality originates from the plasmon–molecule interaction.[101] Maoz et al. reported for instance that non-chiral gold islands coated with riboflavin or polylysine displayed a chiroptical signal close to the plasmon resonance band of the gold, the induced CD
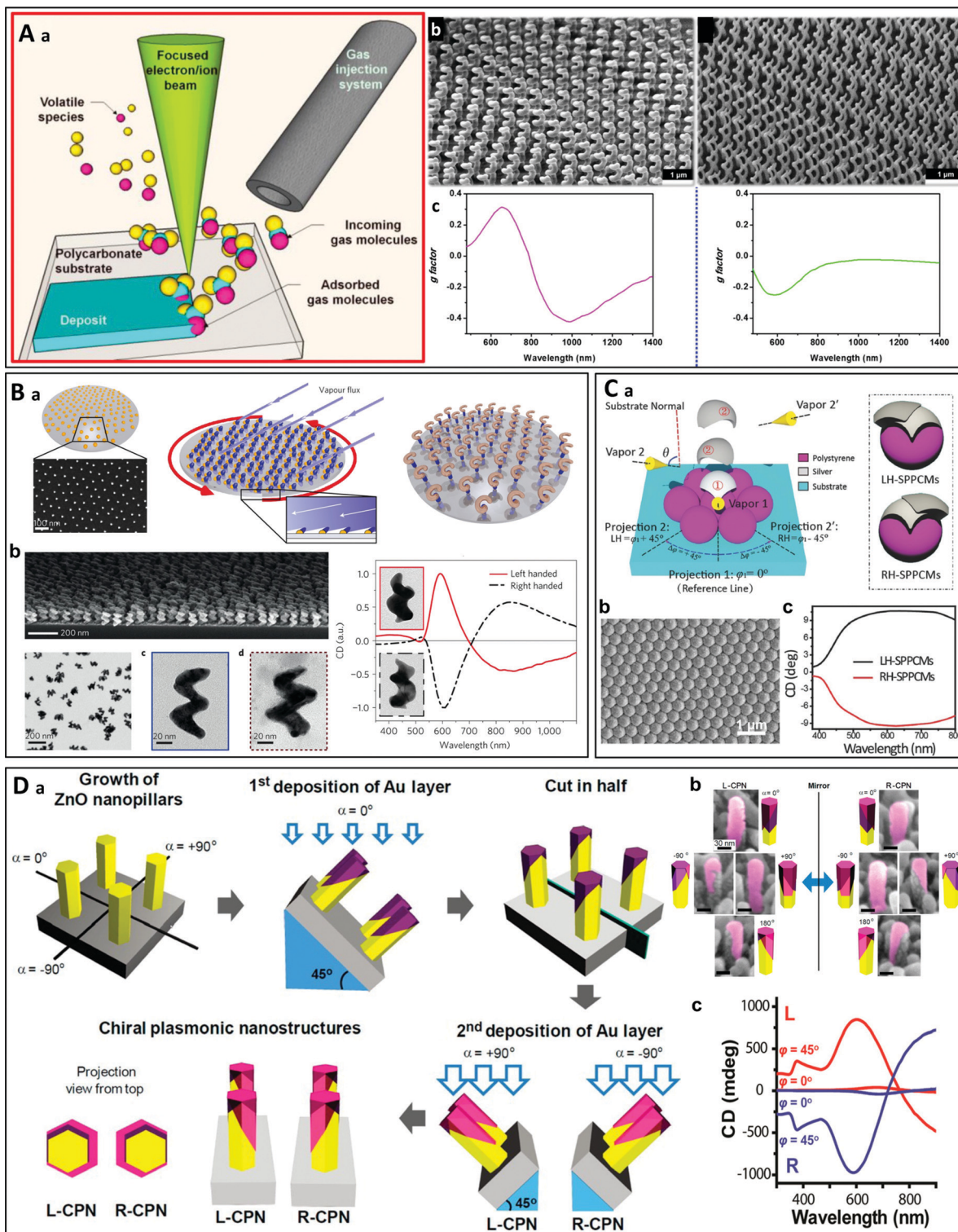
Fig. 3 (A) (a) Schematic principle of FIBID/FEBID on a flexible substrate.[70] Copyright 2015 American Chemical Society. (b) Arrays of chiral platinum nanohelices with different pitches prepared by FIBID (left) and FEBID (right) and (c) their experimental *g*-factor spectra.[71] Copyright 2015 American Chemical Society. (B) (a) Schematic principle of glancing angle deposition (GLAD). (b) SEM images of Au : Cu (65 : 35) nanohelices obtained by GLAD. (c) CD spectra of left- and right-handed Au helices.[73] Copyright 2013 Springer Nature. (C) (a) Schematic representation of two-step GLAD on a self-assembled microsphere monolayer (left) and the resultant LH and RH stacked-patch plasmonic chiral metamaterials (SPPCMs). (b) Top-view SEM image of a 90 nm-thick LH SPPCM. (c) CD spectra of LH and RH SPPCMs.[81] Copyright 2016 John Wiley and Sons. (D) (a) Schematic principle of the synthesis of chiral plasmonic nanoshells (CPNs) by vacuum evaporation. (b) SEM images of the left- and right-handed nanostructures at different angles (Au layers were artificially colored for clarity) and (c) experimental CD spectra of an L-CPN and an R-CPN at normal (*φ* = 0°) and inclined light incidence (*φ* = 45°).[82] Copyright 2013 American Chemical Society.
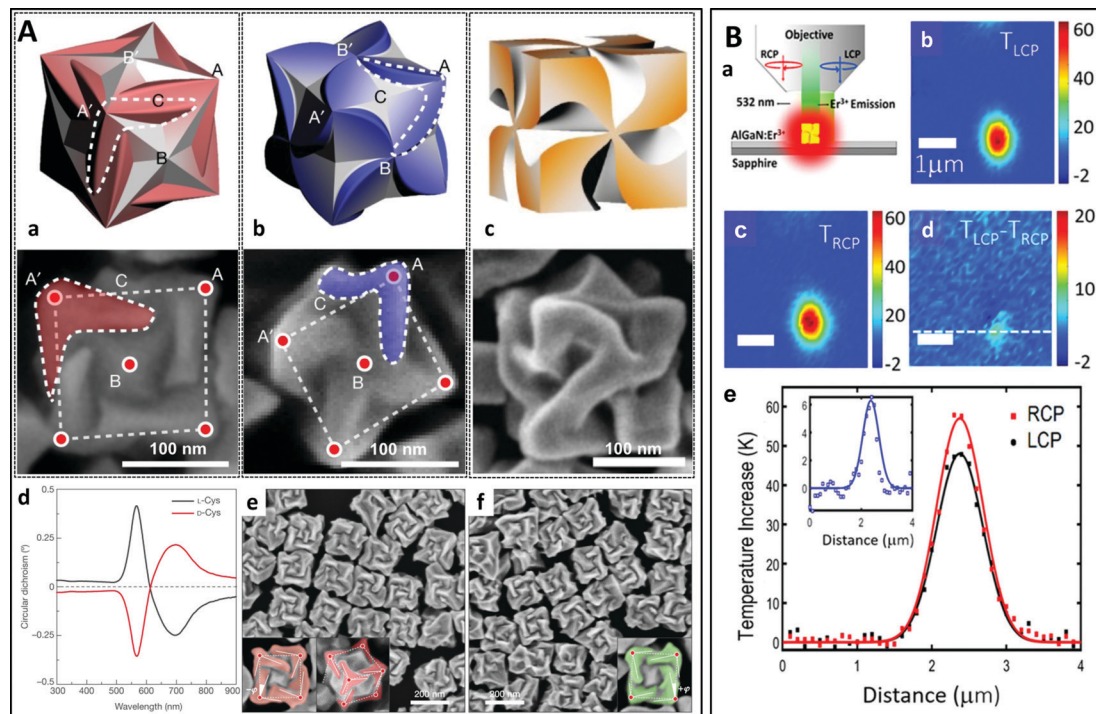
Fig. 4 (A) Chiral gold helicoids obtained by amino-acid- or peptide-directed growth. (a) 432 helicoid I, grown on a cubic seed under L-cysteine-control. (b) 432 helicoid II, grown on a cubic seed under L-glutathione-control. (c) 432 helicoid III, grown on an octahedral seed under L-glutathione-control. (d)–(f) CD spectra (d) and SEM images of the left-handed (e) and right-handed (f) 432 helicoid I.[87] Copyright 2018 Springer Nature. (B) (a) Schematic diagram of photothermal circular dichroism under RCP/LCP light. (b)–(d) Thermal image of a small cluster of chiral helicoid under LCP (b) and RCP (c) light, and the difference between LCP and RCP individual images obtained from luminescence ratio thermometry (d). (e) Thermal profiles under LCP and RCP illumination. The inset shows the thermal profile from panel (d) along the white dashed line.[89] Copyright 2020 American Chemical Society.

decaying within about 10 nm of the surface of the islands (Fig. 6A).[98] In more recent work,[100] non-chiral chromophores were hybridized with double-stranded DNA, which induced bisignate CD signals at the absorbance band of the chromophores (Fig. 6B). Interestingly, after coupling to a plasmonic resonance mode of gold nanorods, the CD signals were reversed and enhanced by one order of magnitude.

Beyond the transfer of chirality to a single nanoparticle, placing a chiral molecule in the gap between two plasmonic nanoparticles can significantly enhance the chiroptical effect due to the stronger electromagnetic field in the gap, also known as a "hotspot". This important enhancement has seen applications in the sensitive detection of chiral molecules, especially biomolecules (see Section 4.5.1). For example, X. Wu et al. reported the ultrasensitive sensing of a protein by encapsulating the molecule in the gap of a heterodimer of gold and silver nanoparticles (Fig. 6C).[102] Although the geometry was not chiral, the presence of the chiral biomolecule in the plasmonic hotspot led to remarkable plasmonic CD. Recently, L. Tian et al. synthesized plasmonic homodimers and heterodimers with a metal–organic molecular cage (MOC) in the hotspot, which then served as a receiver of (chiral) molecules. The authors demonstrated interesting interaction phenomena including enhanced chirality (Fig. 6D), as well as surface-enhanced Raman scattering and plasmonic tuning.[103] L. M. Kneer et al. prepared a two-layer sheet (2LS) DNA origami supporting single-stranded DNA-coated gold nanospheres or nanorods.[104] Transfer of

chirality from the DNA origamis located in the hotspots to the nanoparticles resulted in enhanced CD signals at the plasmonic resonances. Finally, Severoni et al. placed chiral molecules at the tip of gold nanorods assembled into chains, leading to plasmon-enhanced circular dichroism.[105] The role of optical hotspots at the gaps of linear tip-to-tip nanorod assemblies is shown to be the origin of enhancement in the dichroism from chiral molecules. Furthermore, the refractive index rather than the absorption-mediated chiral response of the molecules is responsible for the dichroism in the visible-NIR plasmonic regime, far from the molecule UV absorption resonances.

3.2.3. Self-assembly. The self-assembly[106–109] of nano-objects into functional superstructures has been a dynamic field of research in recent years. Self-assembly methods, which use chemical or physical forces to arrange individual building blocks in well-defined hierarchical ensembles, represent an important component of the bottom-up strategies to fabricate chiral plasmonic nanostructures.[66,110–112] Indeed, self-assembly can be used to arrange non-chiral plasmonic particles in a chiral pattern, where the interactions of the dipole moments of the individual nanoparticles give rise to coupled collective modes with different responses to LCP and RCP light.[66,113–117] Numerous modes can exist in a complex structure and they can be excited and spectrally overlap with one another, producing the complicated CD spectra of chiral plasmonic nano-assemblies. Self-assembly methods nevertheless
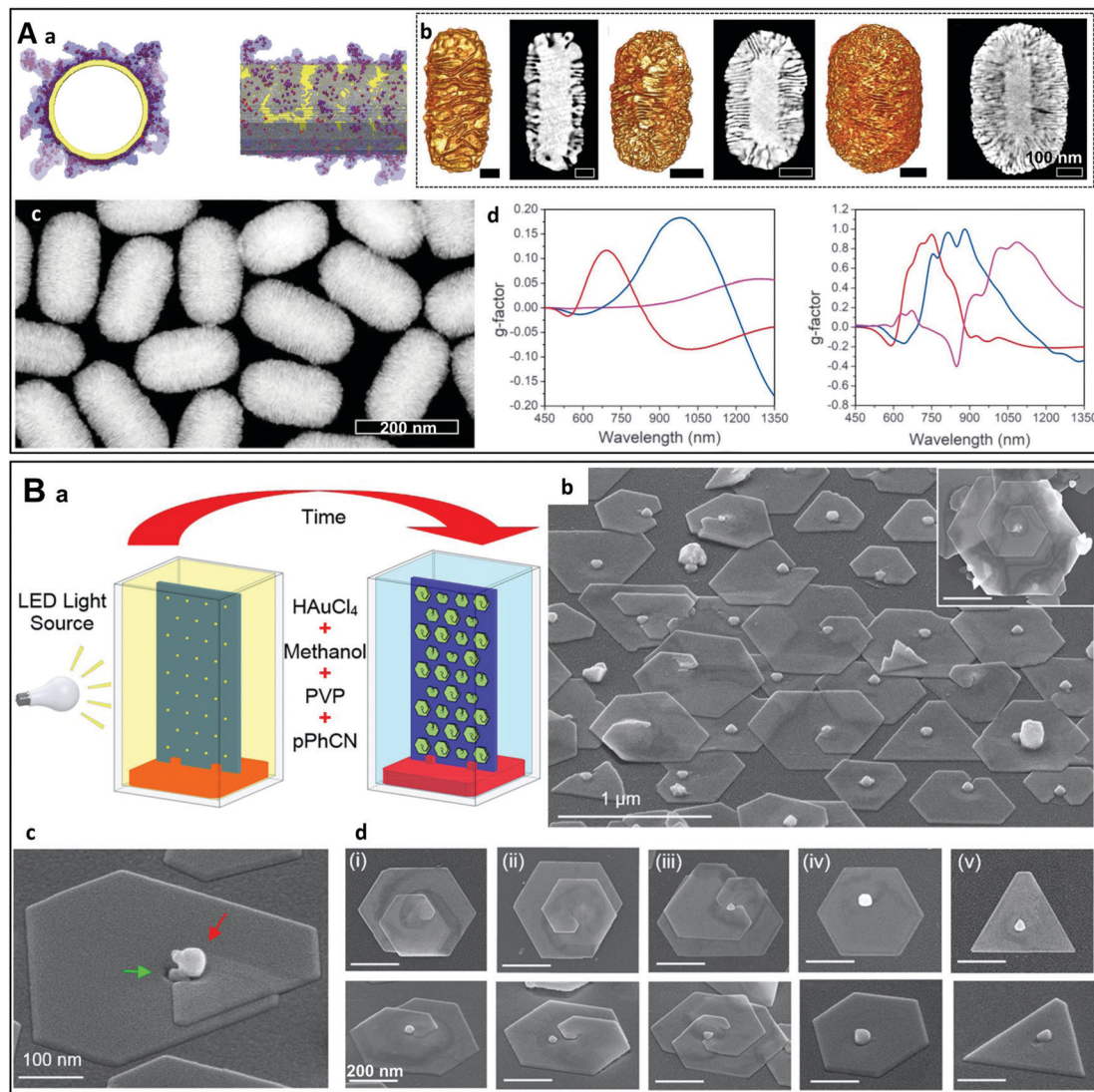
Fig. 5 (A) (a) Axial and lateral views of the molecular dynamic simulation of the structure of a right-handed cosurfactant ((R)-BINOL-CTAC) adsorbed on the surface of a gold nanorod. (b) Tomographic reconstruction and the corresponding HAADF-STEM images of chiral nanorods of three different dimensions (from left to right: 165 × 73 nm, 210 × 112 nm, 270 × 175 nm). (c) High-angle annular dark-field scanning transmission electron microscopy (HAADF-STEM) image at low magnification of gold nanorods obtained in the presence of a right-handed surfactant ((R)-BINAMINE). (d) Measured (right) and simulated (left) g-factors of the chiral gold nanorods of different dimensions (red: 165 × 73 nm, blue: 210 × 112 nm, magenta: 270 × 175 nm).[92] Copyright 2020 The American Association for the Advancement of Science (B) (a) Schematic representation of the experimental set-up used for the light-driven solution-based synthesis of chiral plasmonic nanostructures. (b) SEM images of the chiral nanostructures obtained after 4 hours of reaction. (c) A high-magnification view at a seed location. (d) The five most commonly observed structures display a plate-like morphology.[93] Copyright 2021 American Chemical Society.

provide a very high degree of flexibility in the structural control and thereby allow tailoring of the chiroptical properties through the programmability of the templates or the tunability of the assembly process.[26] Three different ways of obtaining chiral plasmonic nano-assemblies may be distinguished: (1). plasmonic nanoparticles can be grafted onto a pre-existing chiral template, which thus dictates the chiral spatial organization of the nanoparticles; (2). plasmonic nanoparticles can be functionalized with oligomeric scaffolds, which leads to binding of the individual nanoparticles into chiral assemblies through macromolecule-like or supramolecular interactions; (3). physical forces (mechanical stretching, shear forces, light...)

can be applied externally during/after assembly to break the symmetry and induce anisotropy.

3.2.3.1. Nanoparticle assembly on pre-formed chiral templates. Conventional templates for chiral plasmonic assemblies include thin films patterned by e-beam-lithography,[118] polymers,[119,120] nanofibers,[121,122] DNA[98,123–129] and other biomolecules.[130,131] For example, chiral assemblies have been synthesized in aqueous suspensions of plasmonic nanorods using chiral supramolecular nanofibers as templates (Fig. 7A).[121] Jung *et al.* employed a gelator template moiety in combination with specific helicity-directing molecular
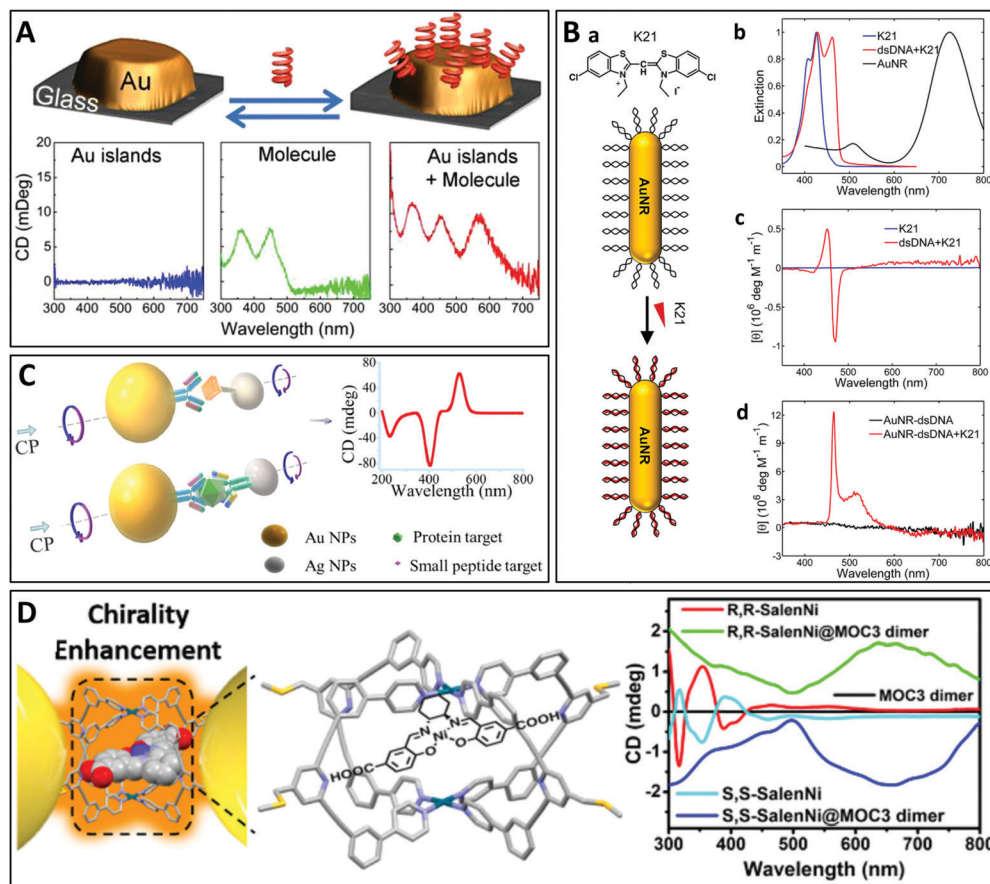
Fig. 6 (A) Chiroptical activity induced by interaction with riboflavin placed close to a non-chiral gold nanoparticle (AuNP). CD emerges at the plasmonic resonance of the AuNP while the CD of the biomolecule is also enhanced.[98] Copyright 2013 American Chemical Society. (B) (a) Schematic representation of the assembly of the chromophore molecule K21 with a gold nanorod (AuNR) conjugated to double-stranded DNA (dsDNA). (b) Normalized extinction spectra of aqueous solutions of K21 before (blue) and after (red) binding to dsDNA and of AuNRs alone (black). (c) CD spectra of K21 before and after binding to dsDNA. (d) CD spectra of AuNRs conjugated to dsDNA before and after self-assembly of K21 on the DNA templates.[100] Copyright 2019 American Chemical Society. (C) Schematic illustration of the assembly of NP heterodimers and their use for biological analyses.[102] Copyright 2013 American Chemical Society. (D) Chirality enhancement of chiral molecules encapsulated in the MOC located in the gap of a plasmonic dimer.[103] Copyright 2021 American Chemical Society.

components to produce long helical nanofibers, on which the controlled growth of gold nanoparticles at spatially arranged locations along the fibers was achieved by UV reduction of Au(ı) ions on the supramolecular templates.[132] Chemical reduction of Au(ı) has also been performed on the supramolecular fibers of chiral peptides.[133–136] In two recent reports, Oda *et al.* described the assembly of gold nanospheres on silica helices through hydrostatic interactions[137] and covalent binding[138] (Fig. 7B). The chiroptical properties arose from anisotropic coupling between the nanoparticles arranged on the helices. This was further evidenced by the fact that the chiral character of the material vanished in a multilayer film of aligned helices when the helices were close enough to interact with each other.[138] Multilayer films of oriented nanoparticle-grafted helices have been aligned using grazing incidence spraying (GIS).[139–143] The multilayer structure was obtained through layer-by-layer (LbL) assembly,[144,145] whereby the interlayer spacing can be finely tuned. When the spacing between the helices is small, non-chiral interactions between nanoparticles

on neighboring helices dominate the chiral interactions between nanoparticles on the same helix, causing loss of the chiroptical properties. This work is one of the examples demonstrating that chiroptical properties can be modulated not only in the individual chiral building blocks but also through hierarchical arrangement using self-assembly methods.

Another strategy employs cellulose nanocrystals which naturally form cholesteric phases. Upon evaporation of a mixed suspension of cellulose and gold nanorods/nanoparticles[131,146–150] or silver nanowires,[151] the nano-objects are embedded during evaporation (Fig. 7C). Chiral soft liquid crystals may also be used to template the assembly of plasmonic nanoparticles.[152–155] These templates can enable the efficient assembly of larger amounts of nano-objects but lack tunability, which is limited by their structure.

The DNA origami represents another very popular template allowing the synthesis of reconfigurable chiral nanostructures.[156–158] This involves the folding of long DNA strands into 2D and 3D nanostructures by hybridizing them with so-called staple oligonucleotides. The staple oligonucleotides are connected with the
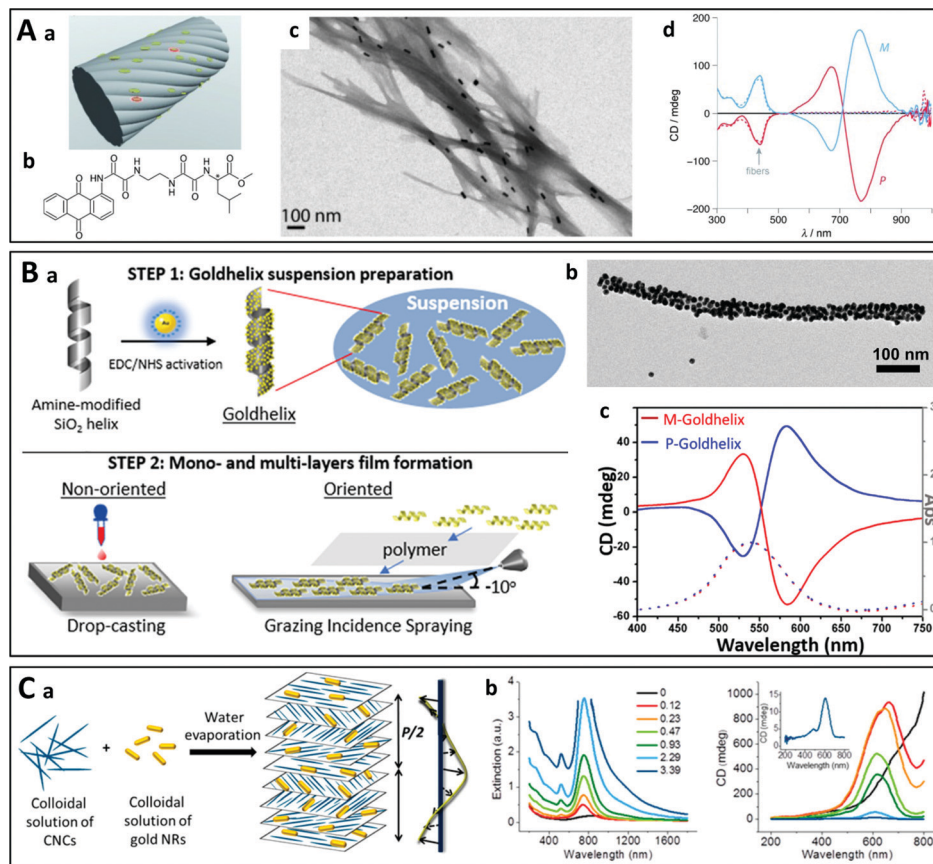
Fig. 7   (A) (a) Schematic representation of the nanoparticles on the supramolecular fibers prepared from anthraquinone-based oxalamide (b). (c) TEM image of gold nanorods adsorbed on twisted supramolecular *M*-fibers. (d) Experimental CD spectra of right- (*P*) and left-handed (*M*) fibers.[121] Copyright 2011 John Wiley and Sons. (B) (a) Schematic principle of the assembly of gold nanoparticles on silica helices and their incorporation into multilayer thin films by LbL assembly. (b) TEM image of a gold-nanoparticle-coated silica helix. (c) CD (solid line) and absorbance (dashed line) of a *P*- and *M*-silica helix coated with gold nanoparticles.[138] Copyright 2020 American Chemical Society. (C) Liquid crystal-like chiral nanostructures obtained by self-assembly of gold nanorods (NRs) and cellulose nanocrystals (CNCs) as the template. Upon slow evaporation of water from an aqueous suspension of a mixture of CNCs and gold NRs, the CNCs form a left-handed liquid crystalline cholesteric phase and the NRs embedded in the cholesteric solid film align with the orientation of the cellulose nanofibers. (b) Extinction (left) and CD spectra (right) with increasing concentration of NRs in the film.[131] Copyright 2014 American Chemical Society.

DNA through Watson–Crick base pairing and their positions are predetermined, which dictates the shape of the DNA origami structures. When used as template for the self-assembly of chiral plasmonic nanostructures,[66,159,160] the DNA origami acts as a scaffold on which the nanoparticles are grafted and is the origin of the chirality.[161] For example, in pioneering work in 2012, long DNA strands bearing hundreds of specifically designed staple oligonucleotides were assembled in a DNA origami containing 24-helix bundles offering nine attachment sites for single-stranded DNA-coated gold nanoparticles.[126] Left-handed and right-handed self-assembled gold helices were thus obtained, leading to a CD close to the resonance wavelength of the individual particles (Fig. 8A). Lan *et al.* used bifacial origamis and gold nanorods (AuNRs) to construct discrete 3D anisotropic plasmonic dimer nanoarchitectures with a precisely modulable spatial configuration.[162] The same group further prepared AuNR helical superstructures with predetermined chirality where the origami was intercalated between neighboring AuNRs.[163]

This approach allowed precise control of the inter-rod distance and angle as well as the average number of nanorods in the helices (Fig. 8B).

Diverse chiral architectures based on DNA origami have been prepared, including gold nanorod dimers[164–167] and trimers,[165,168] gold–silver core–shell nanorod dimers,[169] micrometer-long plasmonic polymers,[170] spherical AuNP tetrahedron architectures.[171] Very recently, Martens *et al.* studied the long- and short-range chiral interactions in DNA-assembled plasmonic chains where the coupling was ensured by an achiral nanosphere situated between a pair of gold nanorods arranged far apart but in a chiral fashion using a DNA origami.[172] The transmitter particle caused strong enhancement of the CD response with the emergence of an additional chiral feature at the resonance frequency of the nanosphere. Lan *et al.* have developed an approach for the tunable self-assembly of chiral DNA supramolecular architectures using a versatile DNA origami adapter.[173] The configurational handedness of self-assembled metastructures of plasmonic nanorods can be

Fig. 8 (A) (a) Schematic representation of left-handed and right-handed gold helices assembled on DNA bundles. (b) TEM image of assembled left-handed gold nanohelices. (c) and (d) Measured (c) and modeled (d) CD spectra of left-handed (red lines) and right-handed (blue lines) helices that are made from 16 nm gold nanoparticles.[126] Copyright 2012 Springer Nature. (B) (a) Schematic representation of the self-assembly of right-handed AuNR helices using a DNA origami. (b) Cryo-TEM images of the assembled AuNR helices containing varying numbers of AuNRs and the corresponding reconstructed models. (c) CD spectra of right-handed and left-handed helices containing varying number of AuNRs. (d) Calculated surface charge distribution profile of a right-handed helix upon induced by the illumination with LCP and RCP light.[163] Copyright 2015 American Chemical Society. (C) (a) Schematic representation of a gold nanorod dimer attached to two DNA bundles at a tunable angle. The CD of the structure can be modulated by adding specific DNA strands to change the angle between the two nanorods. (b) TEM images of the plasmonic metamolecules in the right-handed state. (c) CD spectra measured in the left-handed (red line), relaxed (black line) and right-handed (blue line) states. (d) The plasmonic metamolecules can be driven to either the left- or right-handed state by adding specific DNA strands (R_1 and R_2). The CD signal was monitored over time at a fixed wavelength of 725 nm.[177] Copyright 2014 Springer Nature. (D) (a) Schematic of the plasmonic walker. Two gold nanorods (AuNRs) are assembled perpendicularly to one another on a double-layer DNA origami template, and the walking track comprises six rows of footholds (A–F) to define five walking stations (I–V). (b) Measured CD spectra at different stations. (c) Directional (forward and reverse) nanoscale "walking" of a nanorod on a DNA sheet leads to a change in the CD of the nanorod dimer.[178] Reproduced under the terms and conditions of the CC-BY license.

modulated with the DNA origami adapter to produce stair-like and coil-like metastructures.

Many efforts have been made to design DNA origami-based chiral nanostructures responding to external stimuli,[115,174]

which may be employed for the sensitive detection of (bio)molecular species in solution.[175] Thanks to the reversible binding of the DNA strands, actively tunable chiral plasmonic nanostructures can be obtained using DNA origami templates.[176]

For instance, A. Kuzyk *et al.* prepared gold nanorod dimers supported by and attached to two DNA bundles.[177] By adding specific DNA strands connecting or disconnecting the four arms of the two DNA bundles, it was possible to tune the relative angle between the nanorod dimers and thus the handedness of the structure (Fig. 8C). C. Zhou *et al.* showed that the CD of a nanorod dimer could be changed through directional (forward and reverse) nanoscale "walking" of one of the rods on the two-layer sheet of a DNA origami (Fig. 8D).[178] In another study, Ryssy *et al.* prepared a light-responsive dynamic DNA origami-based plasmonic assembly by using the action of light on a merocyanine-based photoacid to change the pH of the medium. This led to the formation of DNA triplex links, inducing spatial reconfiguration of the plasmonic nanoparticles.[179] Lan *et al.* used rationally designed DNA strand displacement reactions to induce active transformations of the DNA template, modulating the superstructures between a tightly folded state and an extended one of the same handedness, or between two mirror-image states of opposite handedness.[124] Chiral plasmonic nanosystems can also be conjugated with split aptamers, which can respond to both thermal and aptamer-targeted regulation, allowing the detection of specific targets including adenosine triphosphate and cocaine molecules.[180] Jiang *et al.* assembled L-shaped gold nanorod dimers on rhombus-shaped DNA origami templates.[181] The geometry and chiral signals of the AuNR nanoarchitectures responded to multiple stimuli, including glutathione reduction, restriction enzymes, pH change or photoirradiation.

3.2.3.2. Assembly driven by nanoparticle functionalization or chiral molecules. The assembly approaches discussed in the previous section are based on the binding of functionalized nanoparticles to predesigned chiral templates. Another self-assembly strategy depends on the use of nanoparticles functionalized with molecules that will lead to a chiral assembly, or the co-assembly of nanoparticles and chiral molecules which will spontaneously aggregate in a chiral pattern. The chirality is introduced by a chiral molecular species, or by functionalizing the nanoparticles with molecules having specific interactions and hence no previously synthesized chiral template is needed.

Single-stranded DNA (ssDNA) chains are widely used to functionalize nanoparticles on account of their ability to bind very specifically to their complementary ssDNA through DNA hybridization. For example, chiral pyramids[182–184] have been obtained using ssDNA scaffolds (Fig. 9A). Gold nanoparticles of two different sizes were synthesized and functionalized with four different ssDNA strands constituting two complementary pairs. Asymmetric pyramids composed of two large and two small gold nanoparticles were produced by hybridizing the two kinds of functionalized nanoparticles. The same group has prepared gold nanorod dimers as well as twisted assemblies with multiple nanorods in both side-by-side and end-to-end configurations using a DNA polymerase chain reaction.[185] Due to the heat sensitivity of the reaction, similar structures have been shown to respond to temperature changes (Fig. 9B).[186]

The nanorods form chiral dimers upon cooling as DNA assembly occurs, while the chirality vanishes upon heating as a result of DNA disassembly. Asymmetric heterodimers can also be prepared by assembling spherical nanoparticles on a single nanorod.[187,188]

Another group has proposed a "sergeants-and-soldiers" strategy using cysteine molecules at the nanorod tips, acting as sergeants, and surfactant molecules on the nanorod surface, acting as soldiers.[189] During assembly, the surfactants transfer and amplify the local chirality induced by the adsorbed cysteine molecules from the plasmonic monomers to the oligomers composed of a few twisted nanorods. Particles with a much more complex hierarchical organization have been prepared from polydisperse gold thiolate nanoplatelets bearing cysteine surface ligands (Fig. 9B).[190] The intricate organization arises from competing chirality-dependent assembly restrictions which make the assembly pathways primarily dependent on the symmetry rather than the size of the nanoparticles. Depending on the handedness of the cysteine, the particles can form twisted ribbons which then coalesce into more complex structures such as the so-called coccolith-like particles (CLIPs). Interestingly, the gold thiolate nanoribbons of the hierarchically organized particles coated with L-cysteine are right-handed, whereas the stacks of these nanoribbons are left-handed. The handedness of the nanoribbons and their stacks is inversed if D-cysteine is employed. A diversity of complex structures could be obtained by varying the nucleation temperature and enantiomeric excess. A similar approach has also been used to prepare semiconductor helices from CdTe nanoparticles.[191,192]

Gold nanorods-coated by cysteine assemble into structures with diverse geometries. Zhu *et al.* formed for instance end-to-end linear assemblies of cysteine-coated gold nanorods,[193] while Zhao *et al.* built chiral side-by-side assemblies of gold nanorods that are responsive to the optomechanical perturbations exerted by circularly polarized light.[194] The same group recently demonstrated a non-linear amplification of chirality in self-assembled cysteine-coated gold nanorods due to the so-called "majority-rule", which describes the situation where a slight excess of one enantiomer in a mixture of chiral molecular monomers can lead to a strong bias towards the supramolecular helicity of this (major) enantiomeric monomer.[195] The location of the chiral molecule on the nanorod was shown to play a major role,[196] and the chiral nanorod dimers could be coated with silica to increase their stability.[197] Actually, even racemic mixtures of liquid crystals can produce chiral materials on small scales: Szustakiewicz *et al.* showed that the principles of chirality synchronization (a phenomenon known for small molecules, which results in the formation of chiral domains from transiently chiral molecules) could be used to control the co-crystallization of spherical gold nanoparticles and liquid crystal molecules, yielding domains composed of highly ordered helical nanofibers, preferentially twisted to the right or the left within each domain, even though the bulk material was racemic.[198]

Peptides are also frequently employed to stabilize nanoparticles.[87,199–202] The assembly of the nanoparticles is
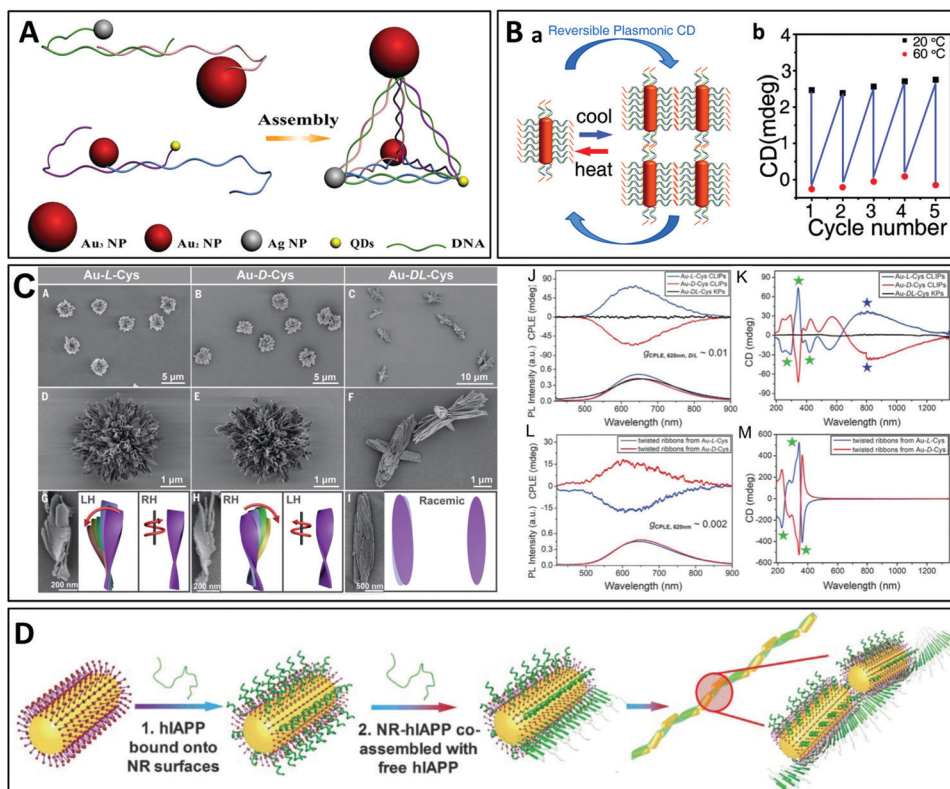
Fig. 9 (A) Nanoparticles functionalized with ssDNA strands are assembled into chiral pyramids by DNA hybridization.[183] Copyright 2012 American Chemical Society. (B) Assembly and disassembly of gold nanorod dimers functionalized with ssDNA strands upon cooling and heating.[186] Copyright 2012 American Chemical Society. (C) Low magnification SEM images of hierarchically organized gold nanoparticles coated with cysteine surface ligands, which formed left- or right-handed coccolith-like particles (CLIPs) [(A) and (B)], or kayak particles (C) when a racemic mixture of D- and L-cysteine was used. (D to F) Enlarged SEM images of Au−L-Cys and Au−D-Cys CLIPs [(D) and (E)] and Au−DL-Cys kayak particles (F). (G to I) SEM images and the corresponding schematic illustrations of the individual twisted ribbons constituting the CLIPs. (J) Circularly polarized light emission (CPLE) and (K) CD spectra of Au−L-Cys CLIPs (blue), Au−D-Cys CLIPs (red) and Au−DL-Cys kayak particles (black). (L) CPLE and (M) CD spectra of Au−L-Cys (blue) and Au−D-Cys (red) twisted ribbons.[190] Copyright 2020 The American Association for the Advancement of Science. (D) Liquid crystal-like helices with a long-range order obtained by assembly of the human islet amyloid polypeptide (hIAPP) with NRs.[199] Copyright 2021 The American Association for the Advancement of Science.

achieved through polymerization of the peptides anchored on the particle surface. In a recent study, J. Lu *et al.* used the human islet amyloid polypeptide (hIAPP) for the helical assembly of gold nanorods (Fig. 9D).[199] The hIAPP is the hormone that regulates physiological glucose concentrations and is responsible for fiber formation in the human brain. Its secondary structure forms a β-sheet which assembles into long tape-like helical structures with a regular pitch. These authors conjugated gold nanorods with hIAPP and obtained liquid crystal-like helices through self-assembly of the peptide β-sheets. The helical assemblies with long range organization displayed a *g*-factor of up to 0.12, which was 4600 times higher than that of the individual nanorods functionalized with hIAPP. The enhanced optical asymmetry stemmed from the long-range coupling of the longitudinal plasmons, while unfavorable scattering was reduced by antiparallel orientation of the dipoles. In addition, geometrical factors such as the nanorod size, helical pitch, distance between the nanorods and number of nanorods could be finely tuned, allowing for tunability of the optical asymmetry. In another recent report, Bhat *et al.* described the synthesis of monodisperse gold nanoparticles

coated with liquid crystalline dimer-like arylamines, which spontaneously assembled into a fluid/frozen lamellar structure exhibiting CD activity.[203] The similar hierarchical, cooperative self-assembly/self-organization of gold nanorods, a micelle-forming surfactant and bilayer-forming amphiphilic phospholipids led to the formation of a chiral liquid crystal-like mesophase.[204] Finally, dual thermal- and photo-switchable plasmonic chiral assemblies have been prepared using a supramolecular approach with gold nanorods modified with guanosine, deoxyguanosine and boric acid, which form a chiral gel upon mixing. Upon heating, the chiral nanofibers disassemble and the chiroptical properties vanish.[205] In another study, chiral cholesterol-capped gold nanoparticles were mixed with two nematic liquid crystal hosts, forming chiral nematic phases.[206] The helical pitch was shown to depend on the nanoparticle size and the number of chiral ligands bound to the nanoparticle surface. Finally, Cheng *et al.* recently showed that gold nanorods can be co-assembled with chiral polymers to form side-by-side helical assemblies.[207]

Although it was not performed with plasmonic particles, a unique example of the light-induced chiral self-assembly of

nanoparticles was reported by J. Yeom et al.[208] The authors used circularly polarized light as a "template" for the chiral self-assembly of CdTe nanoparticles. CdTe nanoparticles may be stabilized with thioglycolic acid (TGA) and are themselves chiral. A racemic dispersion containing equal numbers of left- and right-handed CdTe–TGA nanoparticles was illuminated with chiral light. The left-handed (respectively right-handed) nanoparticles more efficiently absorbed left-handed (respectively right-handed) photons, which caused the photooxidation of TGA and its decomposition. As a result, illumination of the racemic dispersion with circularly polarized light led to an excess of unprotected nanoparticles of the same handedness and their selective assembly into twisted nanoribbons with an enantiomeric excess exceeding 30%. This is one of the rare examples of the translation of chirality from chiral photons to matter and may be an indication of the origin of homochirality on Earth. A similar strategy was applied to gold nanoparticles, but realization of the light-driven synthesis of chiral nanostructures turned out to be more difficult for plasmonic nanoparticles than for the semiconductor due to the short lifetime of the plasmonic states. Illumination of gold salt solutions with circularly polarized light was nevertheless shown to induce the formation of nanoparticles and their subsequent assembly into chiral nanostructures.[209] Despite their seemingly irregular shape, the resulting nanocolloids exhibited CD spectra with opposite polarity upon exposure to photons with left or right circular polarization. In another example, Horrer et al. showed that a perfectly achiral nanostructure exhibits a near-field response that is sensitive to the handedness of light due to near-field interference between the different plasmonic modes sustained by the plasmonic metamolecule under circularly polarized light excitation.[210] The local near-field chirality could be imprinted into a photosensitive polymer film, efficiently transforming the optical chirality into geometrical chirality, the initially achiral structure becoming chiral after interaction with chiral light. Finally, Morisawa et al. irradiated gold nanorods supported on TiO_2 with RCP or LCP light to generate electric fields with a chiral distribution around each nanorod.[211] A photoinduced reversible redox reaction (site-selective oxidation due to plasmon-induced charge separation and reduction by UV-induced TiO_2 photocatalysis) was used to selectively deposit PbO_2 around the nanorods with a chiral geometry.

The self-assembly approaches described above may potentially be scaled-up to produce chiral nanostructures in large amounts, although they are sometimes based on expensive reagents such as long synthetic DNA strands. Furthermore, the tunability is often limited by the molecular template as this dictates the scale on which chirality emerges. Finally, the transfer of these chiral building blocks from suspensions to complex multimaterial metadevices remains a challenge. The use of external forces to synthesize template-free chiral thin films over macroscopic areas has thus been proposed.

3.2.4. Directed self-assembly. An emerging strategy which ensures both tunability and scalability of the targeted nanostructures is to use self-assembly techniques that are already well established for non-chiral systems in combination with an external force. Nanoparticles can be deposited in patterns over large areas using various approaches which do not inherently induce a chiral pattern, but where an external force can be exerted during or after the assembly to break the symmetry.

For example, Choi et al. showed that herringbone-patterned plasmonic sheets with periodic kirigami cuts allowed modulation of the polarization of terahertz radiation in the presence of a mechanical strain (Fig. 10A).[212] The micrometer-scale dimensions of the nanostructure led to chiroptical properties in the terahertz range, but a similar pattern on the nanoscale would lead to chiroptical activity in the visible range.[48] Such kirigami modulators have a huge potential for applications in numerous domains, including polarization-based terahertz imaging, line-of-sight telecommunication, encryption of information and space exploration.[212] In addition, the intensity and handedness of the CD can be actively tuned and/or reversed by mechanical deformation of the kirigami templates. These reconfigurable chiral nanostructures[115] have attracted increasing interest in recent years as they offer dynamic and/or reversible control of the chiroptical properties which can be used in smart nanooptic metamaterials as likewise in molecular motors and open the way to a better understanding of the dynamics of light–matter interaction. Kim et al. reported another example where chirality was induced by application of a mechanical torque during the assembly of achiral gold nanoparticles (Fig. 10B).[213] Gold nanoparticle multilayers were deposited by LbL assembly on a flexible substrate which was mechanically twisted during deposition. This approach is extremely simple as the handedness can be conveniently controlled on the nanoscale in a top-down fashion using macroscale deformation, and the chirality is retained even after releasing the torsion. In addition, the CD of the samples can be reversibly tuned by stretching and releasing the substrates. In another work, thermomechanical strain in a multilayer assembly of spherical gold nanoparticles on a Ti layer patterned by nanoimprint lithography was used to prepare large-area surface-bound 3D chiral meta-atoms arrays.[214] Another example makes use of a helical magnetic field to assemble magnetoplasmonic $Ag@Fe_3O_4$ core–shell nanoparticles into chains stacked in a chiral nematic-like superstructure that can be dynamically modulated at the millisecond time scale.[215]

Chirality can also be obtained by stacking layers of in-plane oriented 1D nano-objects or 1D assemblies with a twist, leading to so-called Bouligand structures. Using a very elegant and simple approach, Probst et al. have recently shown that twisted chiral assemblies can be prepared from spherical gold nanoparticles (Fig. 11B).[216] The nanoparticles were arranged in a striped pattern by capillary-assisted assembly[217–219] using nanochannel templates made by lithography. Parallel arrays of gold nanoparticles on two substrates were stacked face-to-face with a twist, the handedness of the structure being determined by the angle of twist which could be selected at will. Interestingly, the two substrates could be separated and repositioned, while the CD of the structure could be actively modulated by compression of the film. A similar multilayer
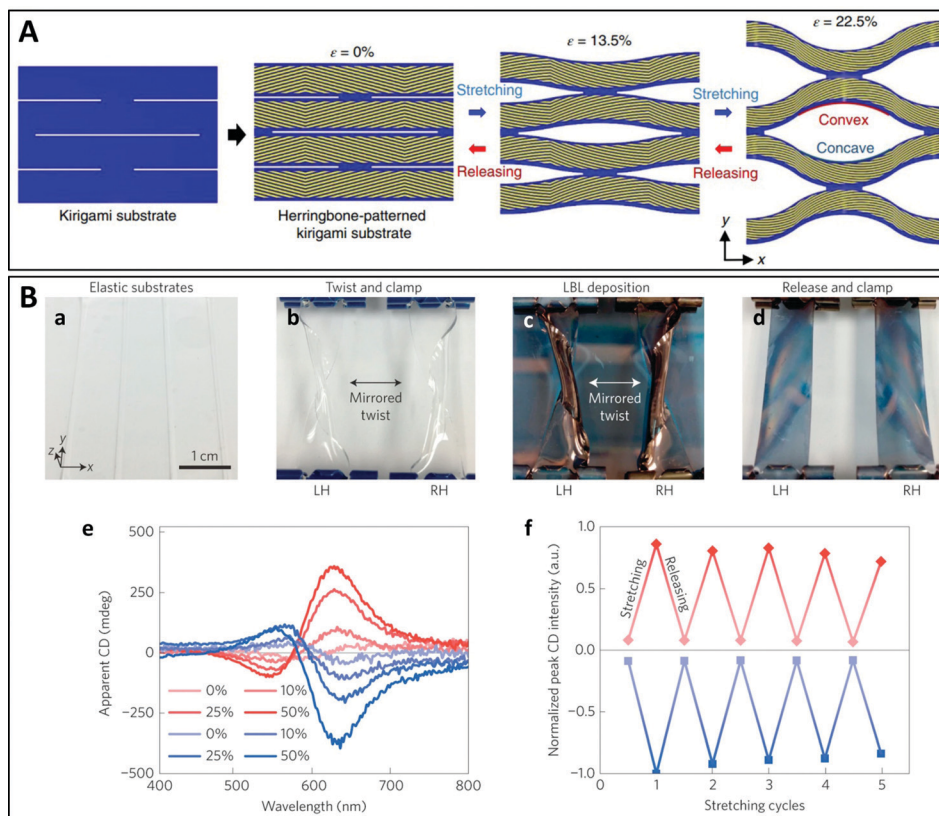
Fig. 10 (A) Schematic representation of a kirigami reconfigurable chiral plasmonic structure: herringbone-patterned gold strips are deposited on the kirigami substrate which can be stretched to modulate the polarization rotation angle and ellipticity.[212] Copyright 2019 Springer Nature. (B) Reconfigurable mechano-tunable chiral metasurfaces obtained by colloidal assembly of spherical gold nanoparticles on a twisted flexible substrate. (a) PDMS substrates. (b) PDMS substrates twisted in opposite directions. (c) LbL deposition of AuNPs on the twisted substrates. (d) Relaxed substrates coated with AuNP multilayers. (e) CD spectra of LH (red) and RH (blue) samples under stretching (from 0% to 50%). (f) Peak CD values of LH and RH samples during five cycles of reversible stretching from 0 to 50%.[213] Copyright 2016 Springer Nature.

twisted architecture was obtained by Hu *et al.*[220] using grazing incidence spraying, a versatile and efficient technique for the alignment of 1D nano-objects in monolayer thin films, which has previously been used to align silver nanowires,[140,142] gold nanorods,[141] cellulose nanofibers,[139] or semiconducting oxide nanowires.[143] Layers of oriented silver nanowires and gold nanorods were incorporated into twisted 2- and 3-layer films using LbL assembly (Fig. 11B).[220] The advantages of this approach are that the number of oriented plasmonic layers, their composition and the angle between them can be freely chosen, and the interlayer spacing may be finely tuned.[221] The thin films displayed broadband CD extending over the UV, visible and near-infrared ranges and reaching extremely high *g*-factors. Finally, Lv *et al.* reported the fabrication of biomimetic chiral photonic crystals (Fig. 11C) consisting of a multilayer twisted stack of aligned inorganic nanowires.[222] This structure mimics the cuticle of many scarabaeoid beetles that are able to selectively reflect left circularly polarized light. The individual layers oriented and deposited using the Langmuir–Schaefer technique and the multilayer structure was obtained by LbL assembly. The high *g*-factors could be modulated by controlling structural parameters of the crystals, including the number of layers, the pitch and the twisting angle.

4. Applications

Chiral plasmonic metamaterials have unique polarization-dependent optical properties that are potentially tunable, which opens up perspectives for applications in polarization-sensitive optical devices such as chiroptical detectors and filters, in 3D displays or to induce chiral forces.[25,63,111] However, it is the possibility of coupling chiral surface plasmons to the metamaterial environment that has driven the research to find applications mostly in molecular sensing,[223,224] enhanced spectroscopies,[225] non-linear chiroptics and chiral catalysis.[226]

4.1. Chiral forces

The interaction of chiral particles with light (which may be chiral or not) can result in a force that depends on the particle handedness and can therefore be used to manipulate and sort the particles. For instance, Wang and Chan predicted that an electromagnetic plane wave should exert a lateral optical force on a chiral particle above a reflective surface, which will emerge as the particle interacts with the reflection of its scattered field.[227] Interestingly, this force acts in a direction where there is neither wave propagation nor an intensity gradient, and deflects particles with opposite helicities towards opposite sides.

Fig. 11 (A) Schematic principle of chiral assembly through macroscopic stacking of achiral linear arrays of spherical gold nanoparticles. (a) The gold particles are assembled into dimer chains in nanochannels. (b) The CD can be dynamically controlled by changing the stacking angle and compression. (c) Photograph demonstrating the polarization-sensitive transmission of LCP or RPC light through a sample stacked at −45°.[216] Copyright 2021 Springer Nature. (B) Twisted multilayer films of oriented silver nanowires (AgNWs). (a) A first layer of oriented AgNWs is deposited by grazing incidence spraying on the substrate, before (b) depositing a multilayer polyelectrolyte dielectric spacer of precisely tunable thickness d by LbL assembly. (c) The next AgNW layer is deposited after rotating the sample through an arbitrary angle. (d) and (e) Top-view and cross-section SEM images of left- and right-handed 2-layer films. (f) The interlayer spacing d can be finely tuned and (g) the corresponding broadband chiroptical properties depend strongly on this spacing.[220,221] Copyright 2021 American Chemical Society. (C) Biomimetic Bouligand nanostructure with modulable chirality obtained by Langmuir−Schafer deposition of inorganic nanowires and LbL assembly. (a) Photographs of *Anomala corpulenta Motschulsky* taken under LCP or RCP light. (b) Cross-section SEM image of the cuticle of *Anomala corpulenta Motschulsky* showing a layered structure. (c) Schema of a chiral photonic crystal with a helical arrangement of layers of aligned NiMoO$_4$·xH$_2$O nanowires. (d) and (e) Schematic principle of the Langmuir−Schaefer deposition of a layer of aligned nanowires. (f) Cross-section SEM image and photograph (inset) of the chiral photonic crystal film obtained by LbL transfer with a predetermined twisting angle.[222] Copyright 2019 John Wiley and Sons.

Hayat *et al.* later showed that lateral forces can be produced by direct interaction of the optical spin angular momentum with chiral particles, pushing them in opposite directions depending on their helicity.[228] This was also investigated in a Kretschmann configuration by Zhang *et al.*[229]

Canaguier-Durand *et al.* have proposed a systematic description of the forces and torques that chiral light fields can exert on chiral objects.[230] In particular, they showed that the chiral force components are directly related to the optical rotation and circular dichroism, and hence that the resulting

forces and torques depend on the enantiomeric form of the chiral dipole, opening up perspectives for the use of chiral light forces to mechanically separate chiral objects according to their enantiomeric form. In a follow-up paper, the same group demonstrated that a plasmonic field propagating on a metal–dielectric interface is able to exert a lateral force on chiral spheres having either optical rotation or circular dichroism.[231] Chiral surface plasmon polaritons possess transverse spin angular momentum with rich and non-trivial characteristics, which leads to the emergence of transverse optical forces in opposite directions for chiral objects of different handedness.[232] These opposite lateral forces acting on two enantiomers of the same size point to the possibility of employing plasmonic fields to manipulate them.

Such chiral forces may be used to optically trap a chiral particle, as demonstrated experimentally and theoretically by the capture of chiral liquid crystal microspheres by circularly polarized Gaussian or Laguerre–Gaussian light beams.[233] Similarly, coaxial plasmonic apertures illuminated with circularly polarized light have been shown to selectively trap enantiomeric dielectric nanoparticles of less than 20 nm.[234] Theory indicated that the interaction of chiral light with chiral objects could be mediated by achiral plasmonic apertures. An alternative system designed by Liu *et al.* to discriminate and separate chiral enantiomers employs tightly focused vector-polarized hollow beams, which possess a transverse spin angular momentum that can rotate the chiral particles along the transverse direction.[235] Linearly polarized light has also been used to sort chiral particles with diameters in the same wavelength range at an air–water interface.[236] The lateral forces arise from a complex interplay between the light polarization, lateral momentum enhancement and out-of-plane light refraction at the particle–water interface.

4.2. Polarization photodetectors

Chiral photodetectors are optoelectronic devices that can detect circularly polarized light and are an important component in next-generation information technology.[237–239] While various approaches have been explored to manipulate circularly polarized light using compact optical elements, the development of an efficient and highly selective photodetector for circularly polarized light which can be integrated into complex photocircuits remains a challenge. Coupling a chiral plasmonic metasurface to a photosensitive material is one strategy that has been investigated in recent years. Jiang *et al.* designed an ultrathin circular polarimeter by coupling a chiral gold nanostructure with a monolayer $MoSe_2$ 2D semiconductor (Fig. 12A).[240] The detector was shown to produce a photocurrent which depended strongly on the circular polarization of the incoming light. A similar device was obtained by coupling a plasmonic chiral metasurface to a TiO_2 film, a wide band gap semiconductor (Fig. 12B).[241] The resulting hybrid structure exhibited different hot electron transfer rates for left-handed and right-handed visible light which could be used to sense the light polarization. Kim *et al.* demonstrated numerically that a circular polarization-sensitive organic photodetector can be designed by coupling an organic photoactive layer

with a chiral plasmonic nanocavity.[242] Another proposed strategy uses an Al_2O_3 layer embedded between two Al layers with a chiral shape to form a p–i–n diode.[243] Circularly polarized light can be even detected directly using the hot electrons produced in a chiral plasmonic metamaterial interfaced with an n-type silicon wafer, which constitutes a Schottky barrier (Fig. 12C).[244]

Instead of measuring a polarization-sensitive photocurrent, the handedness of light can also be detected optically by coupling chiral nano-antennas to a light-emitting dye-doped slab.[245] Furthermore, it has been shown that the photothermal effect of chiral plasmonic nanostructures is polarization-sensitive,[89] which can be exploited to build a circular polarimeter[246] or for enantioselective photothermal imaging.[247] Besides circularly polarized light detection, McCarthy *et al.* recently showed that nanorod dimers could be used to detect trochoidal dichroism (trochoidal field motion being both planar and rotational, producing a cartwheeling motion liked to a significant phase delay between transverse and longitudinal oscillations).[248,249]

4.3. Non-linear chiroptical properties

Non-linear chiroptical effects, such as second-harmonic generation (SHG) circular dichroism (SHG-CD) and optical rotation (SHG-OR) are known to be much more pronounced than their linear optical counterparts.[250] These effects may be particularly intense in plasmonic materials. Ren *et al.* showed for instance that the non-linear optical activity of a plasmonic metamaterial consisting of periodic arrays of asymmetric split ring slits was several orders of magnitude larger than that in naturally occurring inorganic crystals.[251] Similar results were obtained for plasmonic metasurfaces consisting of split-ring resonator meta-atoms[252] or in a helical metamaterial,[36] while Famularo *et al.* were able to measure the non-linear chiroptical response of individual micro-helices by dark-field spectroscopy and non-linear optical microscopy.[253] Chiral-selective non-linear signals could also be used for the high-contrast second-harmonic optical imaging of a micrometer-scale chiral pattern.[254] Ohnoutek *et al.* recently used the newly developed hyper-Rayleigh scattering optical activity (HRS OA) technique to probe the nonlinear chiroptical properties of the gold helicoids described in Fig. 4A.[255] Moreover, the third-harmonic generation (THG) CD of chiral bilayer gold metasurfaces was successfully modeled using a coupled anharmonic oscillator based on chirally coupled electric dipole moments.[57]

While the non-linear optical anisotropy is pronounced in such plasmonic metasurfaces, the intensity of the non-linear optical response is still quite low. This challenge was taken up by Kim *et al.* in recent work using a polaritonic chiral plasmonic cavity coupled with the intersubband transitions of semiconducting heterostructures designed to have giant second and third order non-linear responses.[256] A non-linear circular dichroism of close to unity and conversion efficiencies of over 10^{-4}% for SHG- and THG-CD were achieved simultaneously on a single chip. Similarly, coupling of a 2D van der Waals semiconductor (tungsten disulfide) with an aluminum vortex metalens led to high SHG-CD.[257] THG-CD
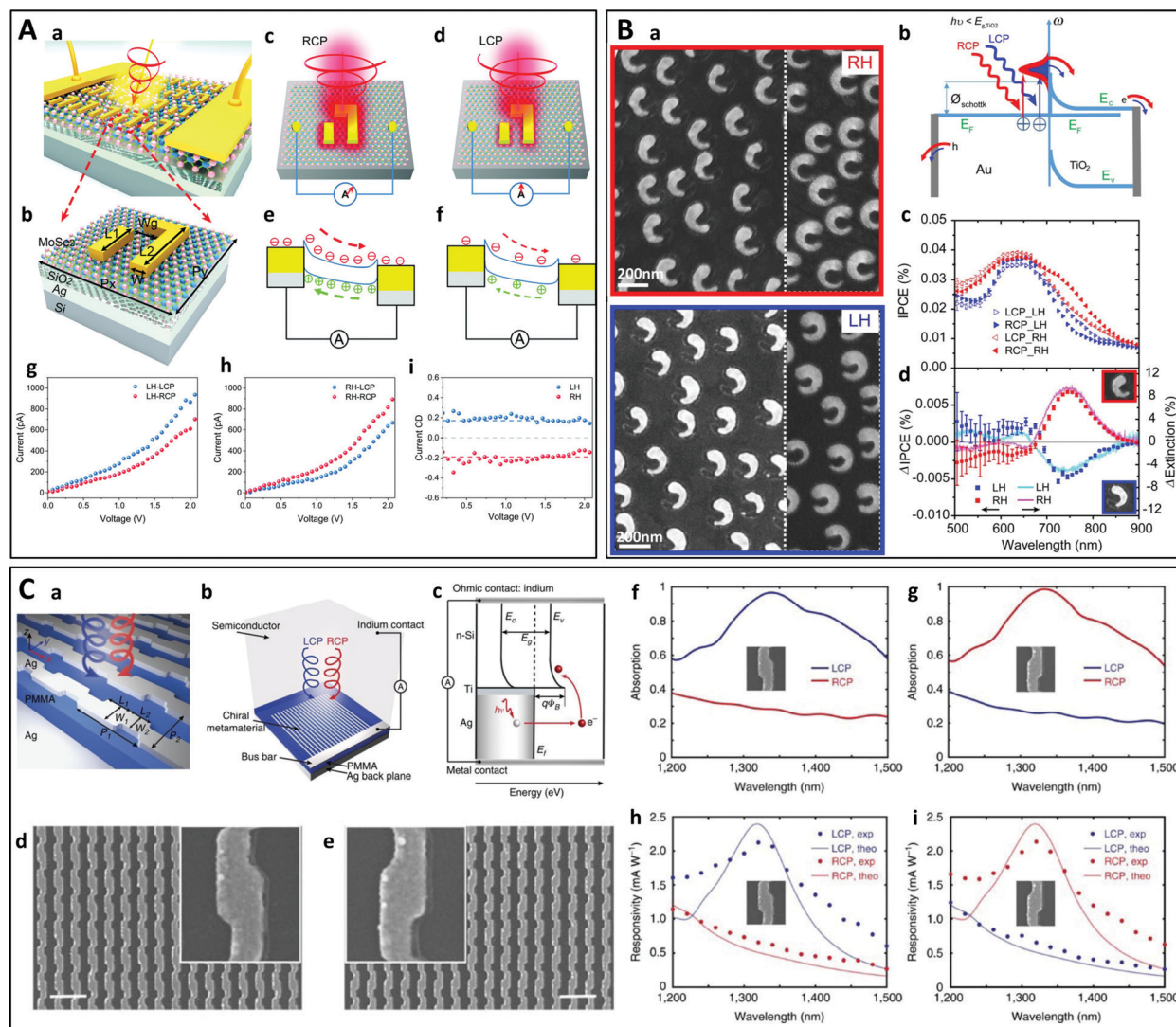
Fig. 12 (A) Chiral plasmonic metasurface on a MoSe$_2$ monolayer. (a) Schematic of the hybrid structure. (b) A unit cell of the chiral plasmonic metasurface. (c) and (d) Schematic of the selective enhancement of electromagnetic field for the RH plasmonic metasurface under illumination of RCP (c) and LCP (d) light. (e) and (f) Energy band diagrams of the device for the RH plasmonic metasurface under illumination of RCP (e) and LCP (f) light, respectively. (g and h) Measured $I–V$ responses for LH (g) and RH (h) metasurfaces under circularly polarized light illumination. (i) Photocurrent CD $vs.$ bias voltage for both handedness.[240] Copyright 2020 The Royal Society of Chemistry. (B) Hot electron generation from chiral gold split-ring-resonators (SRRs) on TiO$_2$ (a) SEM images of SRRs of opposite handedness on TiO$_2$. (b) Schematic illustration of the hot electron transfer process from the chiral SRRs to the TiO$_2$ layer: RCP or LCP light with photon energy below the TiO$_2$ band gap excite plasmons in the chiral SRRs with different efficiency. (c) Incident photon to charge conversion efficiency (IPCE) spectra for RH and LH samples under LCP and RCP illumination. (d) IPCE response difference between RCP and LCP light (ΔIPCE, squares) compared to the circular dichroism (ΔExtinction, full lines) measured for the same samples.[241] Copyright 2016 American Chemical Society. (C) Silver chiral metasurface on a silver backplane separated by a dielectric spacer. (a) Schematic of the device. (b) Schematic of the CPL detector consisting of a chiral metamaterial integrated with a semiconductor that serves as a hot electron acceptor. A Schottky barrier is formed between Si and the Ti interfacial layer. The hot electrons that are photo-generated in the Ag metamaterial are then injected over this barrier into the Si. (d) and (e) SEM images of the LH (d) and RH (e) metamaterial. (f) and (g) Measured optical absorption spectra under LCP (blue) and RCP (red) illumination for LH (f) and RH (g) metamaterials. (h) and (i) Measured (dots) and theoretically calculated (solid curve) photoresponsivity spectra under LCP (blue) and RCP (red) illumination for LH (h) and RH (i) metamaterials.[244] Reproduced under the terms and conditions of the CC-BY license.

with more than an order of magnitude variation between RCP and LCP excitation was also obtained by coupling chiral plasmons to the photonic waveguide mode of a Si layer device.[258]

4.4. Chiral catalysis

Metallic particles are often used as catalysts for chemical reactions,[259,260] but obtaining asymmetric catalysis with

molecular species remains a challenge.[261] Several attempts have been made over the last years to use chiral plasmonic nanoparticles or chiral assemblies of plasmonic particles as enantioselective catalysts.[262] A first approach consisted of templating metal films that are commonly used as electrocatalysts with chiral molecules to produce mesoporous chiral surfaces.[263] Such films were later used by the same group to induce

© 2022 The Author(s). Published by the Royal Society of Chemistry

asymmetry in the electrochemical synthesis of mandelic acid.[264] Starting from a prochiral compound, an excess of the (*R*)-enantiomer when using platinum electrodes templated with (*R*)-molecules was obtained and *vice versa*, while the enantioselectivity could be tuned by changing the number of chiral cavities in the material. A similar approach was employed using nickel electrodes for the discriminatory electro-oxidation of the two phenylethanol enantiomers[265] or using silver electrodes for the electro-oxidation of amino acids.[266] Liu *et al.* prepared Au/Ag alloyed nanotubes coated with cysteine which served as electrodes in an electrochemical cell.[267] Depending on the handedness of the cysteine coat, selective electro-oxidation of tyrosine enantiomers was observed.

Very recently, it was shown that photoinduced reactions performed on chiral plasmonic particles could also result in chiral products.[268] A prochiral molecule, 2-anthracenecarboxylic acid, was stereoselectively adsorbed on Ag and Cu nanohelices as enantiomorphous anti-head-to-head dimers. The dimers displayed either *Si-Si* or *Re-Re* facial stacking depending on the handedness of the nanohelices, which led to a specific enantiopreference during their photoinduced cyclodimerization.

One more example of photoinduced asymmetric synthesis is the crystallization of sodium chlorate. It was initially demonstrated that circularly polarized light could induce a bias during the chiral crystallization of $NaClO_3$.[269] A few years later, Chen *et al.* used non-chiral gold triangle trimers in a saturated solution of sodium chlorate illuminated with RCP or LCP light to obtain a crystalline enantiomeric excess of more than 50%.[270] In a follow-up paper, the same group explained this result by modeling the plasmonic near-field during illumination and showing that the large enantiomeric excess previously observed arose from a difference in the frequency of attachment of chiral crystalline clusters to crystal nuclei, or in the local concentration of $NaClO_3$ due to chirally biased diffusion, rather than from enantioselective optical trapping.[271] A similar light polarization-dependent chiral synthesis was documented using chiral metallic particles, which exhibited a different photocatalytic activity depending on the helicity of the illuminating light.[272] These observations may be explained by considering the different emission rates of hot electrons in chiral plasmonic particles upon illumination with circularly polarized light,[273–275] as experimentally measured by Fang *et al.* in split ring resonators deposited on a semiconductor.[241]

The above studies employed chiral plasmonic systems weakly interacting with their target molecules. It was however recently shown[276–280] that chemical reactions can be controlled through strong light–matter coupling by putting the molecules in cavities.[281] Use of plasmonic chiral cavities[282] could potentially pave the way to enantioselectivity in chemical reactions.

4.5. Sensing

Chiral sensing techniques, in particular CD spectroscopy, have been extensively used to acquire information on biomolecular structures, arrangements and conformations.[223] Although CD is a low-cost and non-invasive approach, the chiroptical signals of biomolecules are usually very weak due to the small characteristic size at which chirality arises as compared to the wavelength of UV or visible light. Various strategies based on plasmonic systems have thus been explored over the last years to enhance the chiroptical signals and the sensitivity of the related biosensing methods.[223,225,283]

4.5.1. Enhancement of the CD of chiral molecules by coupling with non-chiral particles and metasurfaces. The CD of chiral molecules is inherently small due to the different scales of the chiral arrangement of atoms in a molecule and the wavelength of UV or visible light. The use of non-chiral particles or metasurfaces (either metallic[98,101,284] or dielectric,[283,285–287] or a combination of both[288,289]) has been proposed to enhance the local electric field and thereby increase the measured chiroptical signal. In a seminal paper, Govorov *et al.* demonstrated that a non-chiral nanoparticle can modify the CD of a chiral molecule through Coulomb dipole and multipole coupling, resulting in the resonant enhancement of the CD signals of the molecule and also the appearance of new spectral features.[284] A few years later, Maoz *et al.* found that the adsorption of riboflavin or poly-lysine on achiral gold islands induced a CD signal at the wavelength of the surface plasmon resonance.[98] This induction decayed within about 10 nm of the surface of the islands. Nesterov *et al.* investigated numerically the role of plasmon-generated near fields in the enhancement of the CD of chiral molecules placed in the vicinity of plasmonic particles.[101] These authors showed that the relative orientation between the incident light and plasmonic modes played a crucial role and that surprisingly, achiral structures led to greater enhancement than their chiral equivalents.

Another strategy based on the formation of nanoparticle dimers has been described by Xu *et al.*[290] Gold nanoparticles were functionalized with L- or D-cysteine molecules, inducing the formation of nanoparticle dimers with a plasmonic CD signal that depended on the cysteine concentration, reaching a detection limit of 20 pM.

4.5.2. Surface-enhanced Raman optical activity (SEROA) and enantiomer-resolved surface-enhanced Raman scattering (SERS). Raman optical activity (ROA), which measures the difference between the Raman scattering of right- and left-circularly polarized light, was discovered in the early 1970's.[291,292] A big drawback of ROA spectroscopy is the weakness of the signal, the Raman intensity ratio of both circular polarizations being typically of the order of 10^{-4}. Similarly as for surface-enhanced Raman scattering (SERS), it was predicted that the ROA signals of chiral molecules adsorbed on metal surfaces should be strongly increased.[293,294] The experimental proof of this enhancement was only obtained in the 2000's,[295,296] despite the interest of ROA for investigating the structure of biomolecules.[297] Theoretical models were developed to calculate the enhancement of ROA in the case of (off-resonant) chiral molecules placed near plasmonic spherical nanoparticles,[298,299] and it was even predicted that it should be possible to increase the sensitivity of SEROA down to the single-molecule limit on well-designed plasmonic nanostructures.[300] In spite of these predictions and

exciting possibilities, the enhancement achieved in practice by coupling molecules close to plasmonic particles is much weaker.[301–306] Furthermore, Ren *et al.* have shown that depending on the way the molecules adsorb on the metallic particles, all the vibrational modes are not equally enhanced.[302]

An alternative approach employs nanoparticles with a chiral surface or functionalized with chiral linker molecules. For instance, silver colloids functionalized with aromatic linkers were found to form chiral aggregates in the presence of chiral acids, allowing their detection by SEROA.[303] Sun *et al.* used "classical" Raman spectroscopy with chiral gold nanoparticles to detect specific cystine enantiomers.[307] In another study, the surface of a gold grate was functionalized with enantiopure helicene molecules, leading to different SERS signals when it was exposed to L- or D-dihydroxyphenylalanine.[308] Similarly, Liu *et al.* described a chiral plasmonic surface consisting of helical gold fibers which displayed selective SERS factors for different enantiomers.[309]

4.5.3. CD-based sensing using chiral particles and metasurfaces. Chiral plasmonic metasurfaces have been employed to detect chiral[27,77,310–315] and non-chiral[314,316] molecules.

The grafting of alkyl ligands on silver spirals was shown to weaken the experimental chiroptical activity without affecting the CD spectra.[316] Similarly, Jeong *et al.* used optimized AgTi alloy nanohelices to sense changes in the refractive index of the environment (Fig. 13A).[314] These authors showed that not only the amplitudes of the positive and negative maxima in the CD spectra were affected but also the positions of the maxima and the zero-crossing points. Besides this highly sensitive but non-specific detection of a change in the bulk refractive index, biotin-coated helices could also be employed for the specific sensing of avidin.[314] However, most studies of the sensing of biomolecules using chiral plasmonic metasurfaces have been based on the change in the CD spectrum induced by the adsorption of a protein on a chiral gold thin film, according to the pioneering demonstration of Hendry *et al.*[27] In this work, the superchiral electromagnetic fields produced upon excitation of the chiral plasmonic nanostructure were used to detect the adsorption of several proteins down to the picogram scale (Fig. 13B). The same group later demonstrated that these superchiral fields could be employed to investigate the secondary, tertiary and quaternary structure of proteins.[31,310,313] Zhao *et al.*
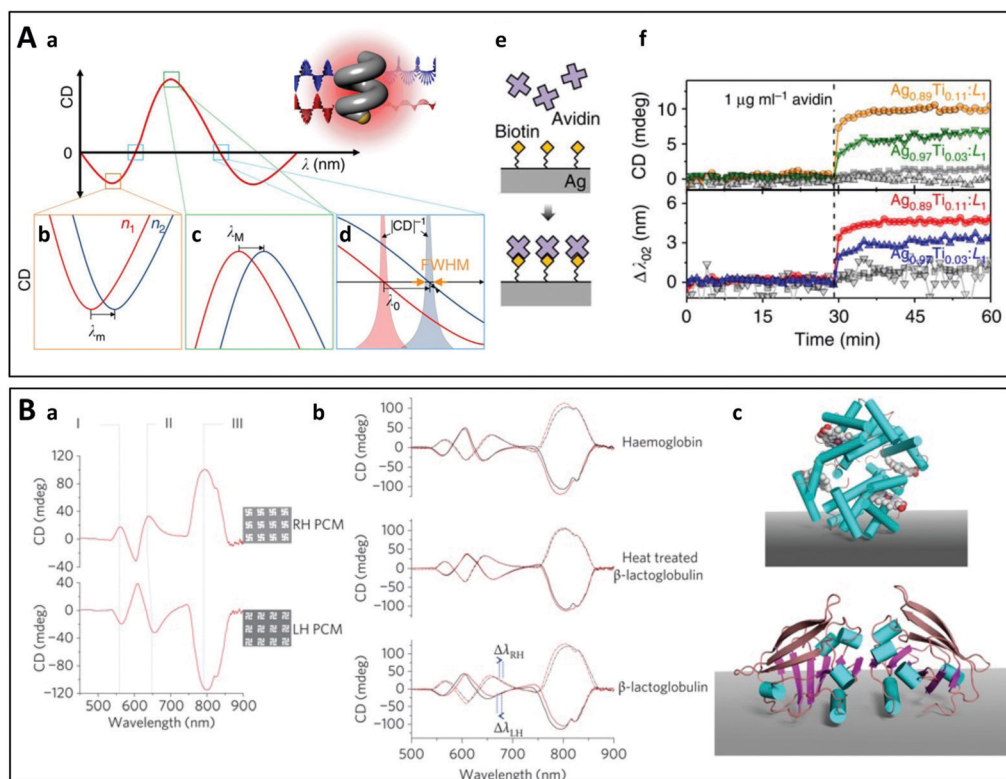

Fig. 13 (A) (a) Schematic principle of polarization-dependent chiral plasmonic sensing using shape-engineered Ag–Ti nanohelices: the CD spectrum of a plasmonic enantiomer is modified when the refractive index of the surrounding medium changes. This modification can be detected at the wavelength of minimum CD λ_m (b), of maximum CD λ_M (c) and at the wavelength at which CD equals zero λ_0 (d). (e) Schematic view of biotin–avidin interaction on the surface of a Ag–Ti nanohelix. (f) *In situ* measurements of the biotin–avidin interaction by monitoring the change of CD at λ_0 and the wavelength shift of $\Delta\lambda_0$ (lower plot) using Ag–Ti nanohelix with different compositions.[314] Reproduced under the terms and conditions of the CC-BY license. (B) (a) CD spectra of the left-handed and right-handed chiral metamaterials immersed in distilled water, and the corresponding SEM images. (b) Influence of the adsorbed proteins haemoglobin, β-lactoglobulin and thermally denatured β-lactoglobulin on the CD spectra of the metamaterials. Red spectra were collected before protein adsorption for the left-handed (solid line) and right-handed (dashed line) metamaterials, and black spectra were collected after protein adsorption. (c) Schematic representation of Haemoglobin (upper) and β-lactoglobulin (lower) shown adopting a well-defined arbitrary structure with respect to a surface.[27] Copyright 2010 Springer Nature.

likewise used the superchiral near-fields generated by plasmonic metasurfaces for biosensing in a flow cell mounted on top of a twisted metamaterial similar to that shown in Fig. 2C,[311] or on a chiral conic nanoshell metallic nanostructure.[77]

Finally, some metals such as palladium and magnesium undergo a fast and reversible phase transition when exposed to hydrogen. This has been used to determine the hydrogen content in the surrounding atmosphere by monitoring changes in the CD of palladium nanohelices[317] or of a chiral metasurface composed of magnesium and gold nanoparticles.[318]

4.5.4. DNA-enabled chiral plasmonic sensing. We previously discussed the high degree of flexibility offered by DNA for the assembly of plasmonic particles into well-defined chiral structures. The unique advantage of this approach is that the DNA nanostructure can be designed to change its shape in response to a specific change in its environment. This geometrical variation can be easily detected in DNA-based chiral assemblies of plasmonic particles using CD spectroscopy,[175] and the highly specific binding between complementary DNA strands has been extensively used to build DNA sensors based on plasmonic DNA superstructures. Thus, chiral plasmonic multimetal nanoparticles of different sizes were functionalized with complementary DNA strands to build chiral heterodimers with a high optical activity.[319] DNA detection at the zeptomolar level was achieved by combining this approach with the exponential amplification of the polymerase chain reaction (PCR) method. Attomolar sensing of DNA without the need for PCR amplification has also been reported using DNA-functionalized nanorods arranged in a side-by-side chiral assembly[185] or post-assembly reconfiguration of nanoparticle pyramids.[320]

DNA-based chiral plasmonic assemblies can even be used for intracellular sensing. In a recent study, Hao *et al.* designed Au@AgAu yolk–shell nanorods with a chiral shape induced by the presence of D/L-penicillamine.[321] Two complementary single-stranded DNAs were attached to the nanorods and to spherical gold nanoparticles. The core–satellite assemblies were generated by DNA hybridization, which led to a change in the CD spectra. These structures were employed to detect Zn^{2+} ions in living cells in the presence of a Zn^{2+}-specific DNA–cleaving DNAzyme. Similarly, microRNA was monitored in living cells by Meng *et al.* using a DNA-driven two-layer core–satellite nanostructure,[322] by Xu *et al.* using side-by-side self-assembly of DNA-functionalized nanorod dimers,[323] and by Li *et al.* using hybrid nanopyramids comprised of gold and upconversion nanoparticles, which allowed them to follow the concentration of microRNA by measuring the plasmonic CD or luminescence.[324]

The high level of control and flexibility offered by DNA origamis has led to their extensive use for CD-based biosensing. Kuzyk *et al.* designed a DNA origami-based reconfigurable plasmonic system which underwent DNA-regulated conformational changes on the nanoscale (Fig. 8C).[177] This group later adapted the same design to sense picomolar amounts of RNA[325] or thrombin by grafting two thrombin-binding aptamers onto the DNA origami.[326] Lan *et al.* similarly designed a left-handed chiral superstructure using gold nanorods and V-shaped DNA origamis.[124] The DNA origamis could be dynamically converted through a toe-hold-mediated strand displacement reaction from a tightly folded state to an extended one, or to the enantiomer (inversion of handedness). The rich DNA chemistry can be used to build complex plasmonic assemblies that switch between different states with detectable changes in the CD spectra, allowing the concomitant sensing of various DNA strands.[178] However, the most widely studied architecture is the cross-shaped assembly of two gold nanorods, which has been employed to detect tumor-marker RNA sequences[327] or different aptamers.[180,328] Beyond its biosensing applications, the same architecture has been used to construct a DNA-based adaptive plasmonic three-state logic gate,[329] with specific input DNA strands coding for three different logic outputs.

5. Conclusions and perspectives

We have outlined in this review the considerable efforts that have been invested over the last years in the design and fabrication of highly efficient chiral materials with targeted properties. Very diverse nanostructures have been prepared ranging from the most simple ones (twisted nanorod dimers) to more complex architectures such as helices, gammadions, or individual nanoparticles with complex chiral symmetries like high-Miller-index helicoid particles.

Several challenges have been at least partially addressed and continue to motivate research in the field. The first is to obtain chiral plasmonic nanostructures with the highest possible chiroptical properties, and the quest for record *g*-factors (highly asymmetric transmittance or scattering/reflectance of RCP and LCP light) is still ongoing. The second is the tunability of the optical properties, especially regarding the wavelength range in which chiroptical properties arise. This necessitates the design of nanostructures with modulable shapes and sizes. The third is the responsiveness to the chemical environment in order to construct active chiral plasmonic systems, which has notably been achieved through DNA origami technology.

Top-down techniques have proven to be particularly effective to produce complex and very well-defined metasurfaces with features of almost arbitrary shape. Unfortunately, although highly efficient to synthesize micrometric structures with chiroptical properties in the THz and infrared domains, these approaches are much more difficult to implement to prepare nanometric structures with chiroptical properties in the visible and UV ranges. The necessary equipment is expensive and the processes are complex, while the structures produced only cover small areas. On the contrary, bottom-up approaches can be easily scaled up (although they may rely on expensive reagents such as artificial DNA) to obtain chiral nanostructures in suspension or in thin films. Chirality may originate from a predesigned chiral template, from assembly/synthesis in the presence of chiral molecules, or in template-free methods from the use of external forces during or after assembly to break the symmetry.

A wide variety of potential applications have been proposed for these novel materials, in particular as optical devices and for sensing applications. Most of these applications are however limited by the high losses inherent to plasmonic nanostructures caused by the resonant excitation of the electron cloud at optical frequencies.[330] These losses induce a huge photothermal effect,[89,247] which is used in some applications such as photothermal therapy.[331,332] This problem has been partly addressed by improving the structure and metal quality[333] or by adding gain materials.[334] However, intrinsic metal losses cannot be avoided, and the use of high-permittivity all-dielectric nanostructures that exhibit very low losses at optical frequencies has been proposed.[335] Their resonances can be utilized in direct analogy to the plasmonic resonances of metallic nanoparticles to engineer their optical response towards specific applications such as sensing.[283,285]

Other challenges in the field of chiral plasmonic metasurfaces will have to be addressed in the coming years. In particular, bridging the gap from the proof-of-concept on a laboratory scale to functional commercial devices will require the design of chiral nanostructures which can be prepared in a reproducible manner on a large scale, can be integrated into more complex multimaterial devices, and retain their properties over long periods under working conditions.

While the structure and properties of these nanomaterials are becoming increasingly well characterized, modeling the structure–property relationships is still a challenge. It is indeed possible to simulate the light–matter interaction on the single nano-object scale using for instance finite difference time domain techniques, but modeling large (chiral) arrays of interacting (chiral) nanoparticles requires powerful computing resources.

Difficulties also persist with regard to the optical characterization of the nano-objects. Far-field chiroptical properties are routinely measured using commercial CD spectrometers, but this technique suffers from many artifacts when employed to characterize anisotropic thin films. This is often neglected and more advanced methods such as Mueller matrix polarimetry are more suited to precisely investigate the intricate polarization characteristics of these complex materials with multiple anisotropies. Furthermore, measuring the chiroptical properties at the level of a single nano-object is one more challenge which should ultimately lead to a better understanding of the near- and far-field properties of these structures.

Finally, the chiral nanostructures that have been studied to date are often quite simple and composed of only one or two different materials, whereas much more complicated hierarchical chiral nanostructures containing multiple materials can be found in nature. The design, fabrication and characterization of such multi-material hierarchical architectures with several levels of anisotropy is a future direction of investigation which will open up new perspectives for fundamental research and practical applications.

Conflicts of interest

There are no conflicts to declare.

Acknowledgements

Notes and references

1 V. Prelog, *Science*, 1976, **193**, 17–24.
2 R. Bentley, *Chirality*, 2010, **22**, 1–2.
3 H. D. Flack, *Acta Crystallogr., Sect. A: Found. Crystallogr.*, 2009, **65**, 371–389.
4 L. Pasteur, *C. R. Hebd. Seances Acad. Sci.*, 1848, **26**, 535–538.
5 J. A. Le Bel, *Bull. Soc. Chim. Fr.*, 1874, **22**, 337–347.
6 J. H. van't Hoff, *Arch. Neerl. Sci. Exactes Nat.*, 1874, **9**, 445–454.
7 J. Bada, *Nature*, 1995, **374**, 594–595.
8 S. Toxvaerd, *Int. J. Mol. Sci.*, 2009, **10**, 1290–1299.
9 A. Salam, *J. Mol. Evol.*, 1991, **33**, 105–113.
10 L. A. Nguyen, H. He and C. Pham-Huy, *Int. J. Biomed. Sci.*, 2006, **2**, 85–100.
11 T. Ito, H. Ando, T. Suzuki, T. Ogura, K. Hotta, Y. Imamura, Y. Yamaguchi and H. Handa, *Science*, 2010, **327**, 1345–1350.
12 A. Mannschreck, R. Kiesswetter and E. von Angerer, *J. Chem. Educ.*, 2007, **84**, 2012.
13 E. Brenna, C. Fuganti and S. Serra, *Tetrahedron: Asymmetry*, 2003, **14**, 1–42.
14 M. H. Boelens, H. Boelens and L. J. Van Gemert, *Perfum. Flavor.*, 1993, **18**, 1.
15 L. Kvittingen, B. J. Sjursnes and R. Schmid, *J. Chem. Educ.*, 2021, **98**, 3600–3607.
16 T. J. Leitereg, D. G. Guadagni, J. Harris, T. R. Mon and R. Teranishi, *J. Agric. Food Chem.*, 1971, **19**, 785–787.
17 M. M. Green and J. V. Selinger, *Science*, 1998, **282**, 879.
18 W. Ma, L. Xu, A. F. de Moura, X. Wu, H. Kuang, C. Xu and N. A. Kotov, *Chem. Rev.*, 2017, **117**, 8041–8093.
19 J. R. Brandt, F. Salerno and M. J. Fuchter, *Nat. Rev. Chem.*, 2017, **1**, 0045.
20 M. Liu, L. Zhang and T. Wang, *Chem. Rev.*, 2015, **115**, 7304–7397.
21 M. Ziegler, A. V. Davis, D. W. Johnson and K. N. Raymond, *Angew. Chem., Int. Ed.*, 2003, **42**, 665–668.
22 N. S. S. Nizar, M. Sujith, K. Swathi, C. Sissa, A. Painelli and K. G. Thomas, *Chem. Soc. Rev.*, 2021, **50**, 11208–11226.
23 F. R. Keene, *Chirality in Supramolecular Assemblies: Causes and Consequences*, John Wiley & Sons, New York, 2016.
24 J. T. Collins, C. Kuppe, D. C. Hooper, C. Sibilia, M. Centini and V. K. Valev, *Adv. Opt. Mater.*, 2017, **5**, 1700182.
25 E. S. A. Goerlitzer, A. S. Puri, J. J. Moses, L. V. Poulikakos and N. Vogel, *Adv. Opt. Mater.*, 2021, **9**, 2100378.
26 M. Hentschel, M. Schäferling, X. Duan, H. Giessen and N. Liu, *Sci. Adv.*, 2017, **3**, e1602735.
27 E. Hendry, T. Carpy, J. Johnston, M. Popland, R. V. Mikhaylovskiy, A. J. Lapthorn, S. M. Kelly, L. D. Barron, N. Gadegaard and M. Kadodwala, *Nat. Nanotechnol.*, 2010, **5**, 783–787.

28 M. Kuwata-Gonokami, N. Saito, Y. Ino, M. Kauranen, K. Jefimovs, T. Vallius, J. Turunen and Y. Svirko, *Phys. Rev. Lett.*, 2005, **95**, 227401.

29 M. Schäferling, D. Dregely, M. Hentschel and H. Giessen, *Phys. Rev. X*, 2012, **8**(2), 031010.

30 O. Arteaga, J. Sancho-Parramon, S. Nichols, B. M. Maoz, A. Canillas, S. Bosch, G. Markovich and B. Kahr, *Opt. Express*, 2016, **24**, 2242–2252.

31 C. Jack, A. S. Karimullah, R. Leyman, R. Tullius, V. M. Rotello, G. Cooke, N. Gadegaard, L. D. Barron and M. Kadodwala, *Nano Lett.*, 2016, **16**, 5806–5814.

32 J. García-Guirado, M. Svedendahl, J. Puigdollers and R. Quidant, *Nano Lett.*, 2018, **18**, 6279–6285.

33 C. Gilroy, S. Hashiyada, K. Endo, A. S. Karimullah, L. D. Barron, H. Okamoto, Y. Togawa and M. Kadodwala, *J. Phys. Chem. C*, 2019, **123**, 15195–15203.

34 J. Kaschke and M. Wegener, *Nanophotonics*, 2016, **5**, 510–523.

35 M. Schäferling, X. Yin, N. Engheta and H. Giessen, *ACS Photonics*, 2014, **1**, 530–537.

36 J. T. Collins, D. C. Hooper, A. G. Mark, C. Kuppe and V. K. Valev, *ACS Nano*, 2018, **12**, 5445–5451.

37 Z. Huang and J. Liu, *Small*, 2017, **13**, 1701883.

38 J. K. Gansel, M. Thiel, M. S. Rill, M. Decker, K. Bade, V. Saile, G. von Freymann, S. Linden and M. Wegener, *Science*, 2009, **325**, 1513–1515.

39 J. K. Gansel, M. Latzel, A. Frölich, J. Kaschke, M. Thiel and M. Wegener, *Appl. Phys. Lett.*, 2012, **100**, 101109.

40 A. Radke, T. Gissibl, T. Klotzbücher, P. V. Braun and H. Giessen, *Adv. Mater.*, 2011, **23**, 3018–3021.

41 M. Thiel, M. S. Rill, G. von Freymann and M. Wegener, *Adv. Mater.*, 2009, **21**, 4680–4682.

42 B. Frank, X. Yin, M. Schäferling, J. Zhao, S. M. Hein, P. V. Braun and H. Giessen, *ACS Nano*, 2013, **7**, 6321–6329.

43 S.-M. Yang, S. G. Jang, D.-G. Choi, S. Kim and H. K. Yu, *Small*, 2006, **2**, 458–475.

44 Z. Wang, B. Ai, H. Möhwald and G. Zhang, *Adv. Opt. Mater.*, 2018, **6**, 1800402.

45 K. M. McPeak, C. D. van Engers, M. Blome, J. H. Park, S. Burger, M. A. Gosálvez, A. Faridi, Y. R. Ries, A. Sahu and D. J. Norris, *Nano Lett.*, 2014, **14**, 2934–2940.

46 K. Dietrich, D. Lehr, C. Helgert, A. Tünnermann and E.-B. Kley, *Adv. Mater.*, 2012, **24**, OP321–OP325.

47 B. Shen, V. Linko, K. Tapio, S. Pikker, T. Lemma, A. Gopinath, K. V. Gothelf, M. A. Kostiainen and J. J. Toppari, *Sci. Adv.*, 2018, **4**, eaap8978.

48 S. Chen, Z. Liu, H. Du, C. Tang, C.-Y. Ji, B. Quan, R. Pan, L. Yang, X. Li, C. Gu, X. Zhang, Y. Yao, J. Li, N. X. Fang and J. Li, *Nat. Commun.*, 2021, **12**, 1299.

49 Y. Guan, Z. Wang, B. Ai, C. Chen, W. Zhang, Y. Wang and G. Zhang, *ACS Appl. Mater. Interfaces*, 2020, **12**, 50192–50202.

50 C. Kuppe, X. Zheng, C. Williams, A. W. A. Murphy, J. T. Collins, S. N. Gordeev, G. A. E. Vandenbosch and V. K. Valev, *Nanoscale Horiz.*, 2019, **4**, 1056–1062.

51 Z. Wu and Y. Zheng, *Adv. Opt. Mater.*, 2017, **5**, 1700034.

52 M. Decker, M. Ruther, C. E. Kriegler, J. Zhou, C. M. Soukoulis, S. Linden and M. Wegener, *Opt. Lett.*, 2009, **34**, 2501–2503.

53 N. Liu, H. Liu, S. Zhu and H. Giessen, *Nat. Photonics*, 2009, **3**, 157–162.

54 Y. Zhao, M. A. Belkin and A. Alù, *Nat. Commun.*, 2012, **3**, 870.

55 M. Decker, R. Zhao, C. M. Soukoulis, S. Linden and M. Wegener, *Opt. Lett.*, 2010, **35**, 1593–1595.

56 Y. Cui, L. Kang, S. Lan, S. Rodrigues and W. Cai, *Nano Lett.*, 2014, **14**, 1021–1025.

57 L. Gui, M. Hentschel, J. Defrance, J. Krauth, T. Weiss and H. Giessen, *ACS Photonics*, 2019, **6**, 3306–3314.

58 X. Yin, M. Schäferling, B. Metzger and H. Giessen, *Nano Lett.*, 2013, **13**, 6238–6243.

59 M. Hentschel, M. Schäferling, T. Weiss, N. Liu and H. Giessen, *Nano Lett.*, 2012, **12**, 2542–2547.

60 M. Liu, E. Plum, H. Li, S. Li, Q. Xu, X. Zhang, C. Zhang, C. Zou, B. Jin, J. Han and W. Zhang, *Adv. Funct. Mater.*, 2021, **31**, 2010249.

61 G. Hu, M. Wang, Y. Mazor, C.-W. Qiu and A. Alù, *Trends Chem.*, 2021, **3**, 342–358.

62 Z. Wu, X. Chen, M. Wang, J. Dong and Y. Zheng, *ACS Nano*, 2018, **12**, 5030–5041.

63 Z. Wang, F. Cheng, T. Winsor and Y. Liu, *Nanotechnology*, 2016, **27**, 412001.

64 M. J. Urban, C. Shen, X.-T. Kong, C. Zhu, A. O. Govorov, Q. Wang, M. Hentschel and N. Liu, *Annu. Rev. Phys. Chem.*, 2019, **70**, 275–299.

65 X.-T. Kong, L. V. Besteiro, Z. Wang and A. O. Govorov, *Adv. Mater.*, 2020, **32**, 1801790.

66 M. J. Urban, C. Shen, X.-T. Kong, C. Zhu, A. O. Govorov, Q. Wang, M. Hentschel and N. Liu, *Annu. Rev. Phys. Chem.*, 2019, **70**, 275–299.

67 M. Hwang and B. Yeom, *Chem. Mater.*, 2021, **33**, 807–817.

68 W. F. van Dorp and C. W. Hagen, *J. Appl. Phys.*, 2008, **104**, 081301.

69 S. J. Randolph, J. D. Fowlkes and P. D. Rack, *Crit. Rev. Solid State Mater. Sci.*, 2006, **31**, 55–89.

70 P. Peinado, S. Sangiao and J. M. De Teresa, *ACS Nano*, 2015, **9**, 6139–6146.

71 M. Esposito, V. Tasco, M. Cuscunà, F. Todisco, A. Benedetti, I. Tarantini, M. D. Giorgi, D. Sanvitto and A. Passaseo, *ACS Photonics*, 2015, **2**, 105–114.

72 Y. Hou, S. Li, Y. Su, X. Huang, Y. Liu, L. Huang, Y. Yu, F. Gao, Z. Zhang and J. Du, *Langmuir*, 2013, **29**, 867–872.

73 A. G. Mark, J. G. Gibbs, T.-C. Lee and P. Fischer, *Nat. Mater.*, 2013, **12**, 802–807.

74 U. Kilic, M. Hilfiker, A. Ruder, R. Feder, E. Schubert, M. Schubert and C. Argyropoulos, *Adv. Funct. Mater.*, 2021, **31**, 2010329.

75 Y. Hou, H. M. Leung, C. T. Chan, J. Du, H. L.-W. Chan and D. Y. Lei, *Adv. Funct. Mater.*, 2016, **26**, 7807–7816.

76 Z. Huang and F. Bai, *Nanoscale*, 2014, **6**, 9401–9409.

77 Y. Qu, Y. Bai, T. Aba, H. Ullah, A. Abudukelimu, J. Huang, T. Gou, J. Li and Z. Zhang, *J. Phys. Chem. C*, 2020, **124**, 13912–13919.

78 T. Wang, T. Fu, Y. Chen and Z. Zhang, *Opt. Lett.*, 2017, **42**, 2842–2845.

79 H. M. Luong, M. T. Pham, T. D. Nguyen and Y. Zhao, *J. Phys. Chem. C*, 2021, **125**, 716–723.

80 S. Sarkar, R. O. Behunin and J. G. Gibbs, *Nano Lett.*, 2019, **19**, 8089–8096.

81 Y. Hou, H. M. Leung, C. T. Chan, J. Du, H. L.-W. Chan and D. Y. Lei, *Adv. Funct. Mater.*, 2016, **26**, 7807–7816.

82 B. Yeom, H. Zhang, H. Zhang, J. I. Park, K. Kim, A. O. Govorov and N. A. Kotov, *Nano Lett.*, 2013, **13**, 5277–5283.

83 Z. Fan and A. O. Govorov, *Nano Lett.*, 2012, **12**, 3283–3289.

84 G. Zheng, J. He, V. Kumar, S. Wang, I. Pastoriza-Santos, J. Pérez-Juste, L. M. Liz-Marzán and K.-Y. Wong, *Chem. Soc. Rev.*, 2021, **50**, 3738–3754.

85 S. W. Im, H.-Y. Ahn, R. M. Kim, N. H. Cho, H. Kim, Y.-C. Lim, H.-E. Lee and K. T. Nam, *Adv. Mater.*, 2020, **32**, 1905758.

86 Y. Ma, Z. Cao, J. Hao, J. Zhou, Z. Yang, Y. Yang and J. Wei, *J. Phys. Chem. C*, 2020, **124**, 24306–24314.

87 H.-E. Lee, H.-Y. Ahn, J. Mun, Y. Y. Lee, M. Kim, N. H. Cho, K. Chang, W. S. Kim, J. Rho and K. T. Nam, *Nature*, 2018, **556**, 360–365.

88 N. H. Cho, G. H. Byun, Y.-C. Lim, S. W. Im, H. Kim, H.-E. Lee, H.-Y. Ahn and K. T. Nam, *ACS Nano*, 2020, **14**, 3595–3602.

89 A. Rafiei Miandashti, L. Khosravi Khorashad, M. E. Kordesch, A. O. Govorov and H. H. Richardson, *ACS Nano*, 2020, **14**, 4188–4195.

90 H.-E. Lee, R. M. Kim, H.-Y. Ahn, Y. Y. Lee, G. H. Byun, S. W. Im, J. Mun, J. Rho and K. T. Nam, *Nat. Commun.*, 2020, **11**, 263.

91 H. Kim, S. W. Im, N. H. Cho, D. H. Seo, R. M. Kim, Y.-C. Lim, H.-E. Lee, H.-Y. Ahn and K. T. Nam, *Angew. Chem., Int. Ed.*, 2020, **59**, 12976–12983.

92 G. González-Rubio, J. Mosquera, V. Kumar, A. Pedrazo-Tardajos, P. Llombart, D. M. Solís, I. Lobato, E. G. Noya, A. Guerrero-Martínez, J. M. Taboada, F. Obelleiro, L. G. MacDowell, S. Bals and L. M. Liz-Marzán, *Science*, 2020, **368**, 1472.

93 S. D. Golze, S. Porcu, C. Zhu, E. Sutter, P. C. Ricci, E. C. Kinzel, R. A. Hughes and S. Neretina, *Nano Lett.*, 2021, **21**, 2919–2925.

94 G. Zheng, Z. Bao, J. Pérez-Juste, R. Du, W. Liu, J. Dai, W. Zhang, L. Y. S. Lee and K.-Y. Wong, *Angew. Chem., Int. Ed.*, 2018, **57**, 16452–16457.

95 A. O. Govorov, Z. Fan, P. Hernandez, J. M. Slocik and R. R. Naik, *Nano Lett.*, 2010, **10**, 1374–1382.

96 H. Behar-Levy, O. Neumann, R. Naaman and D. Avnir, *Adv. Mater.*, 2007, **19**, 1207–1211.

97 T. Levi-Belenkova, A. O. Govorov and G. Markovich, *J. Phys. Chem. C*, 2016, **120**, 12751–12756.

98 B. M. Maoz, Y. Chaikin, A. B. Tesler, O. Bar Elli, Z. Fan, A. O. Govorov and G. Markovich, *Nano Lett.*, 2013, **13**, 1203–1209.

99 F. Lu, Y. Tian, M. Liu, D. Su, H. Zhang, A. O. Govorov and O. Gang, *Nano Lett.*, 2013, **13**, 3145–3151.

100 X. Lan, X. Zhou, L. A. McCarthy, A. O. Govorov, Y. Liu and S. Link, *J. Am. Chem. Soc.*, 2019, **141**, 19336–19341.

101 M. L. Nesterov, X. Yin, M. Schäferling, H. Giessen and T. Weiss, *ACS Photonics*, 2016, **3**, 578–583.

102 X. Wu, L. Xu, L. Liu, W. Ma, H. Yin, H. Kuang, L. Wang, C. Xu and N. A. Kotov, *J. Am. Chem. Soc.*, 2013, **135**, 18629–18636.

103 L. Tian, C. Wang, H. Zhao, F. Sun, H. Dong, K. Feng, P. Wang, G. He and G. Li, *J. Am. Chem. Soc.*, 2021, **143**, 8631–8638.

104 L. M. Kneer, E.-M. Roller, L. V. Besteiro, R. Schreiber, A. O. Govorov and T. Liedl, *ACS Nano*, 2018, **12**, 9110–9115.

105 E. Severoni, S. Maniappan, L. M. Liz-Marzán, J. Kumar, F. J. García de Abajo and L. Galantini, *ACS Nano*, 2020, **14**, 16712–16722.

106 G. M. Whitesides and B. Grzybowski, *Science*, 2002, **295**, 2418–2421.

107 S. Gwo, H.-Y. Chen, M.-H. Lin, L. Sun and X. Li, *Chem. Soc. Rev.*, 2016, **45**, 5672–5716.

108 A. Klinkova, R. M. Choueiri and E. Kumacheva, *Chem. Soc. Rev.*, 2014, **43**, 3976–3991.

109 S. Lee, K. Sim, S. Y. Moon, J. Choi, Y. Jeon, J.-M. Nam and S.-J. Park, *Adv. Mater.*, 2021, 2007668.

110 Z. Cao, H. Gao, M. Qiu, W. Jin, S. Deng, K.-Y. Wong and D. Lei, *Adv. Mater.*, 2020, **32**, 1907151.

111 Z. Chen and X. Lu, *Nano Express*, 2020, **1**, 032002.

112 S. Mokashi-Punekar, Y. Zhou, S. C. Brooks and N. L. Rosi, *Adv. Mater.*, 2020, **32**, 1905975.

113 A. Guerrero-Martínez, J. L. Alonso-Gómez, B. Auguié, M. M. Cid and L. M. Liz-Marzán, *Nano Today*, 2011, **8**(6), 381–400.

114 A. Ben-Moshe, B. M. Maoz, A. O. Govorov and G. Markovich, *Chem. Soc. Rev.*, 2013, **42**, 7028–7041.

115 F. Neubrech, M. Hentschel and N. Liu, *Adv. Mater.*, 2020, **32**, 1905640.

116 L. Hu, T. Liedl, K. Martens, Z. Wang and A. O. Govorov, *ACS Photonics*, 2019, **6**, 749–756.

117 X. Lu, W. Ye, W. You, H. Xie, Z. Hang, Y. Lai and W. Ni, *Phys. Rev. B*, 2020, **101**, 045431.

118 N. J. Greybush, V. Pacheco-Peña, N. Engheta, C. B. Murray and C. R. Kagan, *ACS Nano*, 2019, **13**, 1617–1624.

119 E. Yashima, K. Maeda and T. Nishimura, *Chem. – Eur. J.*, 2004, **10**, 42–51.

120 J. George, S. Kar, E. S. Anupriya, S. M. Somasundaran, A. D. Das, C. Sissa, A. Painelli and K. G. Thomas, *ACS Nano*, 2019, **13**, 4392–4401.

121 A. Guerrero-Martínez, B. Auguié, J. L. Alonso-Gómez, Z. Džolić, S. Gómez-Graña, M. Žinić, M. M. Cid and L. M. Liz-Marzán, *Angew. Chem., Int. Ed.*, 2011, **50**, 5499–5503.

122 M. Golla, S. K. Albert, S. Atchimnaidu, D. Perumal, N. Krishnan and R. Varghese, *Angew. Chem., Int. Ed.*, 2019, **58**, 3865–3869.

123 W. Ma, H. Kuang, L. Wang, L. Xu, W.-S. Chang, H. Zhang, M. Sun, Y. Zhu, Y. Zhao, L. Liu, C. Xu, S. Link and N. A. Kotov, *Sci. Rep.*, 2013, **3**, 1934.

124 X. Lan, T. Liu, Z. Wang, A. O. Govorov, H. Yan and Y. Liu, *J. Am. Chem. Soc.*, 2018, **140**, 11763–11770.

125 A. Cecconello, L. V. Besteiro, A. O. Govorov and I. Willner, *Nat. Rev. Mater.*, 2017, **2**, 17039.

126 A. Kuzyk, R. Schreiber, Z. Fan, G. Pardatscher, E.-M. Roller, A. Högele, F. C. Simmel, A. O. Govorov and T. Liedl, *Nature*, 2012, **483**, 311–314.

127 A. Cecconello, J. S. Kahn, C.-H. Lu, L. Khosravi Khorashad, A. O. Govorov and I. Willner, *J. Am. Chem. Soc.*, 2016, **138**, 9895–9901.

128 T. Man, W. Ji, X. Liu, C. Zhang, L. Li, H. Pei and C. Fan, *ACS Nano*, 2019, **13**, 4826–4833.

129 Y. Zhao and C. Xu, *Adv. Mater.*, 2020, **32**, 1907880.

130 J. M. Slocik, A. O. Govorov and R. R. Naik, *Nano Lett.*, 2011, **11**, 701–705.

131 A. Querejeta-Fernández, G. Chauve, M. Methot, J. Bouchard and E. Kumacheva, *J. Am. Chem. Soc.*, 2014, **136**, 4788–4793.

132 S. H. Jung, J. Jeon, H. Kim, J. Jaworski and J. H. Jung, *J. Am. Chem. Soc.*, 2014, **136**, 6446–6452.

133 A. D. Merg, J. Slocik, M. G. Blaber, G. C. Schatz, R. Naik and N. L. Rosi, *Langmuir*, 2015, **31**, 9492–9501.

134 A. D. Merg, J. C. Boatz, A. Mandal, G. Zhao, S. Mokashi-Punekar, C. Liu, X. Wang, P. Zhang, P. C. A. van der Wel and N. L. Rosi, *J. Am. Chem. Soc.*, 2016, **138**, 13655–13663.

135 S. Mokashi-Punekar, S. C. Brooks, C. D. Hogan and N. L. Rosi, *Biochemistry*, 2021, **60**, 1044–1049.

136 S. Mokashi-Punekar, T. R. Walsh and N. L. Rosi, *J. Am. Chem. Soc.*, 2019, **141**, 15710–15716.

137 J. Cheng, G. Le Saux, J. Gao, T. Buffeteau, Y. Battie, P. Barois, V. Ponsinet, M.-H. Delville, O. Ersen, E. Pouget and R. Oda, *ACS Nano*, 2017, **11**, 3806–3818.

138 J. Gao, W. Wu, V. Lemaire, A. Carvalho, S. Nlate, T. Buffeteau, R. Oda, Y. Battie, M. Pauly and E. Pouget, *ACS Nano*, 2020, **14**, 4111–4121.

139 R. Blell, X. Lin, T. Lindström, M. Ankerfors, M. Pauly, O. Felix and G. Decher, *ACS Nano*, 2017, **11**, 84–94.

140 H. Hu, M. Pauly, O. Felix and G. Decher, *Nanoscale*, 2017, **9**, 1307–1314.

141 S. Sekar, V. Lemaire, H. Hu, G. Decher and M. Pauly, *Faraday Discuss.*, 2016, **191**, 373–389.

142 P. T. Probst, S. Sekar, T. A. F. König, P. Formanek, G. Decher, A. Fery and M. Pauly, *ACS Appl. Mater. Interfaces*, 2018, **10**, 3046–3057.

143 M. Taner Camci, M. Pauly, C. Lefevre, C. Bouillet, M. Maaloum, G. Decher and D. Martel, *Nanoscale*, 2021, **13**, 8958–8965.

144 G. Decher, *Science*, 1997, **277**, 1232–1237.

145 J. J. Richardson, J. Cui, M. Björnmalm, J. A. Braunger, H. Ejima and F. Caruso, *Chem. Rev.*, 2016, **116**, 14828–14867.

146 A. Lukach, H. Thérien-Aubin, A. Querejeta-Fernández, N. Pitch, G. Chauve, M. Méthot, J. Bouchard and E. Kumacheva, *Langmuir*, 2015, **31**, 5033–5041.

147 H. Therien-Aubin, A. Lukach, N. Pitch and E. Kumacheva, *Nanoscale*, 2015, **7**, 6612–6618.

148 H. Thérien-Aubin, A. Lukach, N. Pitch and E. Kumacheva, *Angew. Chem., Int. Ed.*, 2015, **54**, 5618–5622.

149 G. Chu, X. Wang, H. Yin, Y. Shi, H. Jiang, T. Chen, J. Gao, D. Qu, Y. Xu and D. Ding, *ACS Appl. Mater. Interfaces*, 2015, **7**, 21797–21806.

150 A. Querejeta-Fernández, B. Kopera, K. S. Prado, A. Klinkova, M. Methot, G. Chauve, J. Bouchard, A. S. Helmy and E. Kumacheva, *ACS Nano*, 2015, **9**, 10377–10385.

151 G. Chu, X. Wang, T. Chen, J. Gao, F. Gai, Y. Wang and Y. Xu, *ACS Appl. Mater. Interfaces*, 2015, **7**, 11863–11870.

152 D. P. N. Gonçalves, M. E. Prévôt, Ş. Üstünel, T. Ogolla, A. Nemati, S. Shadpour and T. Hegmann, *Liq. Cryst. Rev.*, 2021, **9**, 1–34.

153 S. Shadpour, J. P. Vanegas, A. Nemati and T. Hegmann, *ACS Omega*, 2019, **4**, 1662–1668.

154 L. Bergquist and T. Hegmann, *ChemNanoMat*, 2017, **3**, 863–868.

155 A. Nemati, S. Shadpour, L. Querciagrossa, T. Mori, C. Zannoni and T. Hegmann, *ACS Nano*, 2019, **13**, 10312–10326.

156 P. W. K. Rothemund, *Nature*, 2006, **440**, 297–302.

157 S. M. Douglas, H. Dietz, T. Liedl, B. Högberg, F. Graf and W. M. Shih, *Nature*, 2009, **459**, 414–418.

158 A. Cecconello and F. C. Simmel, *Small*, 2019, **15**, 1805419.

159 J. Ou, H. Tan, X. Chen and Z. Chen, *Nanomaterials*, 2018, **8**, 994.

160 C. Zhou, X. Duan and N. Liu, *Acc. Chem. Res.*, 2017, **50**, 2906–2914.

161 X. Shen, C. Song, J. Wang, D. Shi, Z. Wang, N. Liu and B. Ding, *J. Am. Chem. Soc.*, 2012, **134**, 146–149.

162 X. Lan, Z. Chen, G. Dai, X. Lu, W. Ni and Q. Wang, *J. Am. Chem. Soc.*, 2013, **135**, 11441–11444.

163 X. Lan, X. Lu, C. Shen, Y. Ke, W. Ni and Q. Wang, *J. Am. Chem. Soc.*, 2015, **137**, 457–462.

164 Z. Chen, X. Lan, Y.-C. Chiu, X. Lu, W. Ni, H. Gao and Q. Wang, *ACS Photonics*, 2015, **2**, 392–397.

165 C. Shen, X. Lan, X. Lu, W. Ni and Q. Wang, *Chem. Commun.*, 2015, **51**, 13627–13629.

166 Q. Liu, A. Kuzyk, M. Endo and I. I. Smalyukh, *Opt. Lett.*, 2019, **44**, 2831–2834.

167 O. Ávalos-Ovando, L. V. Besteiro, A. Movsesyan, G. Markovich, T. Liedl, K. Martens, Z. Wang, M. A. Correa-Duarte and A. O. Govorov, *Nano Lett.*, 2021, **21**, 7298–7308.

168 Z. Chen, C. K. K. Choi and Q. Wang, *ACS Appl. Mater. Interfaces*, 2018, **10**, 26835–26840.

169 L. Nguyen, M. Dass, M. F. Ober, L. V. Besteiro, Z. M. Wang, B. Nickel, A. O. Govorov, T. Liedl and A. Heuer-Jungemann, *ACS Nano*, 2020, **14**, 7454–7461.

170 P. Wang, J.-H. Huh, H. Park, D. Yang, Y. Zhang, Y. Zhang, J. Lee, S. Lee and Y. Ke, *Nano Lett.*, 2020, **20**, 8926–8932.

171 G. Dai, X. Lu, Z. Chen, C. Meng, W. Ni and Q. Wang, *ACS Appl. Mater. Interfaces*, 2014, **6**, 5388–5392.

172 K. Martens, F. Binkowski, L. Nguyen, L. Hu, A. O. Govorov, S. Burger and T. Liedl, *Nat. Commun.*, 2021, **12**, 2025.

173 X. Lan, Z. Su, Y. Zhou, T. Meyer, Y. Ke, Q. Wang, W. Chiu, N. Liu, S. Zou, H. Yan and Y. Liu, *Angew. Chem., Int. Ed.*, 2017, **56**, 14632–14636.

174 M.-K. Nguyen and A. Kuzyk, *ACS Nano*, 2019, **13**, 13615–13619.

175 M. Dass, F. N. Gür, K. Kołątaj, M. J. Urban and T. Liedl, *J. Phys. Chem. C*, 2021, **125**, 5969–5981.

176 M. Wang, J. Dong, C. Zhou, H. Xie, W. Ni, S. Wang, H. Jin and Q. Wang, *ACS Nano*, 2019, **13**, 13702–13708.

177 A. Kuzyk, R. Schreiber, H. Zhang, A. O. Govorov, T. Liedl and N. Liu, *Nat. Mater.*, 2014, **13**, 862–866.

178 C. Zhou, X. Duan and N. Liu, *Nat. Commun.*, 2015, **6**, 8102.

179 J. Ryssy, A. K. Natarajan, J. Wang, A. J. Lehtonen, M.-K. Nguyen, R. Klajn and A. Kuzyk, *Angew. Chem., Int. Ed.*, 2021, **60**, 5859–5863.

180 C. Zhou, L. Xin, X. Duan, M. J. Urban and N. Liu, *Nano Lett.*, 2018, **18**, 7395–7399.

181 Q. Jiang, Q. Liu, Y. Shi, Z.-G. Wang, P. Zhan, J. Liu, C. Liu, H. Wang, X. Shi, L. Zhang, J. Sun, B. Ding and M. Liu, *Nano Lett.*, 2017, **17**, 7125–7130.

182 W. Chen, A. Bian, A. Agarwal, L. Liu, H. Shen, L. Wang, C. Xu and N. A. Kotov, *Nano Lett.*, 2009, **9**, 2153–2159.

183 W. Yan, L. Xu, C. Xu, W. Ma, H. Kuang, L. Wang and N. A. Kotov, *J. Am. Chem. Soc.*, 2012, **134**, 15114–15121.

184 A. J. Mastroianni, S. A. Claridge and A. P. Alivisatos, *J. Am. Chem. Soc.*, 2009, **131**, 8455–8459.

185 W. Ma, H. Kuang, L. Xu, L. Ding, C. Xu, L. Wang and N. A. Kotov, *Nat. Commun.*, 2013, **4**, 2689.

186 Z. Li, Z. Zhu, W. Liu, Y. Zhou, B. Han, Y. Gao and Z. Tang, *J. Am. Chem. Soc.*, 2012, **134**, 3322–3325.

187 C. Hao, L. Xu, W. Ma, L. Wang, H. Kuang and C. Xu, *Small*, 2014, **10**, 1805–1812.

188 B. Liu, C. Song, D. Zhu, X. Wang, M. Zhao, Y. Yang, Y. Zhang, S. Su, J. Shi, J. Chao, H. Liu, Y. Zhao, C. Fan and L. Wang, *Small*, 2017, **13**, 1603991.

189 D. Meng, X. Li, X. Gao, C. Zhang, Y. Ji, Z. Hu, L. Ren and X. Wu, *Nanoscale*, 2021, **13**, 9678–9685.

190 W. Jiang, Z. Qu, P. Kumar, D. Vecchio, Y. Wang, Y. Ma, J. H. Bahng, K. Bernardino, W. R. Gomes, F. M. Colombari, A. Lozada-Blanco, M. Veksler, E. Marino, A. Simon, C. Murray, S. R. Muniz, A. F. de Moura and N. A. Kotov, *Science*, 2020, **368**, 642.

191 J. Yan, W. Feng, J.-Y. Kim, J. Lu, P. Kumar, Z. Mu, X. Wu, X. Mao and N. A. Kotov, *Chem. Mater.*, 2020, **32**, 476–488.

192 W. Feng, J.-Y. Kim, X. Wang, H. A. Calcaterra, Z. Qu, L. Meshi and N. A. Kotov, *Sci. Adv.*, 2017, **3**, e1601159.

193 Z. Zhu, W. Liu, Z. Li, B. Han, Y. Zhou, Y. Gao and Z. Tang, *ACS Nano*, 2012, **6**, 2326–2332.

194 W. Zhao, W. Zhang, R.-Y. Wang, Y. Ji, X. Wu and X. Zhang, *Adv. Funct. Mater.*, 2019, **29**, 1900587.

195 M. Song, L. Tong, S. Liu, Y. Zhang, J. Dong, Y. Ji, Y. Guo, X. Wu, X. Zhang and R.-Y. Wang, *ACS Nano*, 2021, **15**, 5715–5724.

196 S. Hou, H. Zhang, J. Yan, Y. Ji, T. Wen, W. Liu, Z. Hu and X. Wu, *Phys. Chem. Chem. Phys.*, 2015, **17**, 8187–8193.

197 B. Han, L. Shi, X. Gao, J. Guo, K. Hou, Y. Zheng and Z. Tang, *Nano Res.*, 2016, **9**, 451–457.

198 P. Szustakiewicz, N. Kowalska, D. Grzelak, T. Narushima, M. Góra, M. Bagiński, D. Pociecha, H. Okamoto, L. M. Liz-Marzán and W. Lewandowski, *ACS Nano*, 2020, **14**, 12918–12928.

199 J. Lu, Y. Xue, K. Bernardino, N.-N. Zhang, W. R. Gomes, N. S. Ramesar, S. Liu, Z. Hu, T. Sun, A. F. de Moura, N. A. Kotov and K. Liu, *Science*, 2021, **371**, 1368–1374.

200 C. Song, M. G. Blaber, G. Zhao, P. Zhang, H. C. Fry, G. C. Schatz and N. L. Rosi, *Nano Lett.*, 2013, **13**, 3256–3261.

201 H.-E. Lee, H.-Y. Ahn, J. Lee and K. T. Nam, *ChemNanoMat*, 2017, **3**, 685–697.

202 Y. Wang, X. Yang, T. Liu, Z. Li, D. Leskauskas, G. Liu and J. B. Matson, *J. Am. Chem. Soc.*, 2020, **142**, 9158–9162.

203 S. A. Bhat, D. S. S. Rao, S. K. Prasad and C. V. Yelamaggad, *Nanoscale Adv.*, 2021, **3**, 2269–2279.

204 R.-Y. Wang, H. Wang, X. Wu, Y. Ji, P. Wang, Y. Qu and T.-S. Chung, *Soft Matter*, 2011, **7**, 8370–8375.

205 S. Wang, Y. Zhang, X. Qin, L. Zhang, Z. Zhang, W. Lu and M. Liu, *ACS Nano*, 2020, **14**, 6087–6096.

206 A. Sharma, T. Mori, H.-C. Lee, M. Worden, E. Bidwell and T. Hegmann, *ACS Nano*, 2014, **8**, 11966–11976.

207 G. Cheng, D. Xu, Z. Lu and K. Liu, *ACS Nano*, 2019, **13**, 1479–1489.

208 J. Yeom, B. Yeom, H. Chan, K. W. Smith, S. Dominguez-Medina, J. H. Bahng, G. Zhao, W.-S. Chang, S.-J. Chang, A. Chuvilin, D. Melnikau, A. L. Rogach, P. Zhang, S. Link, P. Král and N. A. Kotov, *Nat. Mater.*, 2015, **14**, 66–72.

209 J.-Y. Kim, J. Yeom, G. Zhao, H. Calcaterra, J. Munn, P. Zhang and N. Kotov, *J. Am. Chem. Soc.*, 2019, **141**, 11739–11744.

210 A. Horrer, Y. Zhang, D. Gérard, J. Béal, M. Kociak, J. Plain and R. Bachelot, *Nano Lett.*, 2020, **20**, 509–516.

211 K. Morisawa, T. Ishida and T. Tatsuma, *ACS Nano*, 2020, **14**, 3603–3609.

212 W. J. Choi, G. Cheng, Z. Huang, S. Zhang, T. B. Norris and N. A. Kotov, *Nat. Mater.*, 2019, **18**, 820–826.

213 Y. Kim, B. Yeom, O. Arteaga, S. Jo Yoo, S.-G. Lee, J.-G. Kim and N. A. Kotov, *Nat. Mater.*, 2016, **15**, 461–468.

214 J. Guo, J.-Y. Kim, M. Zhang, H. Wang, A. Stein, C. B. Murray, N. A. Kotov and C. R. Kagan, *ACS Nano*, 2020, **14**, 1427–1435.

215 K.-J. Jeong, D. K. Lee, V. T. Tran, C. Wang, J. Lv, J. Park, Z. Tang and J. Lee, *ACS Nano*, 2020, **14**, 7152–7160.

216 P. T. Probst, M. Mayer, V. Gupta, A. M. Steiner, Z. Zhou, G. K. Auernhammer, T. A. F. König and A. Fery, *Nat. Mater.*, 2021, **20**, 1024–1028.

217 S. Ni, L. Isa and H. Wolf, *Soft Matter*, 2018, **14**, 2978–2995.

218 V. Flauraud, M. Mastrangeli, G. D. Bernasconi, J. Butet, D. T. L. Alexander, E. Shahrabi, O. J. F. Martin and J. Brugger, *Nat. Nanotechnol.*, 2017, **12**, 73–80.

219 S. Ni, J. Leemann, I. Buttinoni, L. Isa and H. Wolf, *Sci. Adv.*, 2016, **2**, e1501779.

220 H. Hu, S. Sekar, W. Wu, Y. Battie, V. Lemaire, O. Arteaga, L. V. Poulikakos, D. J. Norris, H. Giessen, G. Decher and M. Pauly, *ACS Nano*, 2021, **15**, 13653–13661.

221 W. Wu, Y. Battie, V. Lemaire, G. Decher and M. Pauly, *Nano Lett.*, 2021, **21**, 8298–8303.

222 J. Lv, D. Ding, X. Yang, K. Hou, X. Miao, D. Wang, B. Kou, L. Huang and Z. Tang, *Angew. Chem., Int. Ed.*, 2019, **58**, 7783.

223 Y. Y. Lee, R. M. Kim, S. W. Im, M. Balamurugan and K. T. Nam, *Nanoscale*, 2020, **12**, 58–66.

224 C. Hao, L. Xu, H. Kuang and C. Xu, *Adv. Mater.*, 2020, **32**, 1802075.

225 X. Mu, L. Hu, Y. Cheng, Y. Fang and M. Sun, *Nanoscale*, 2021, **13**, 581–601.

226 J. Liu, L. Yang, P. Qin, S. Zhang, K. K. L. Yung and Z. Huang, *Adv. Mater.*, 2021, 2005506.

227 S. B. Wang and C. T. Chan, *Nat. Commun.*, 2014, **5**, 3307.

228 A. Hayat, J. P. B. Mueller and F. Capasso, *Proc. Natl. Acad. Sci. U. S. A.*, 2015, **112**, 13190.

229 Q. Zhang, J. Li and X. Liu, *Phys. Chem. Chem. Phys.*, 2019, **21**, 1308–1314.

230 A. Canaguier-Durand, J. A. Hutchison, C. Genet and T. W. Ebbesen, *New J. Phys.*, 2013, **15**, 123037.

231 A. Canaguier-Durand and C. Genet, *J. Opt.*, 2015, **18**, 015007.

232 M. H. Alizadeh and B. M. Reinhard, *ACS Photonics*, 2015, **2**, 1780–1788.

233 G. Tkachenko and E. Brasselet, *Nat. Commun.*, 2014, **5**, 4491.

234 Y. Zhao, A. A. E. Saleh and J. A. Dionne, *ACS Photonics*, 2016, **3**, 304–309.

235 X. Liu, J. Li, Q. Zhang and M. G. Dirbeba, *Phys. Chem. Chem. Phys.*, 2019, **21**, 15339–15345.

236 Y. Shi, T. Zhu, T. Zhang, A. Mazzulla, D. P. Tsai, W. Ding, A. Q. Liu, G. Cipparrone, J. J. Sáenz and C.-W. Qiu, *Light: Sci. Appl.*, 2020, **9**, 62.

237 Z. Ji, W. Liu, S. Krylyuk, X. Fan, Z. Zhang, A. Pan, L. Feng, A. Davydov and R. Agarwal, *Science*, 2020, **368**, 763–767.

238 J. Lin, J. B. Mueller, Q. Wang, G. Yuan, N. Antoniou, X.-C. Yuan and F. Capasso, *Science*, 2013, **340**, 331–334.

239 L. Li, J. Wang, L. Kang, W. Liu, L. Yu, B. Zheng, M. L. Brongersma, D. H. Werner, S. Lan, Y. Shi, Y. Xu and X. Wang, *ACS Nano*, 2020, **14**, 16634–16642.

240 Q. Jiang, B. Du, M. Jiang, D. Liu, Z. Liu, B. Li, Z. Liu, F. Lin, X. Zhu and Z. Fang, *Nanoscale*, 2020, **12**, 5906–5913.

241 Y. Fang, R. Verre, L. Shao, P. Nordlander and M. Käll, *Nano Lett.*, 2016, **16**, 5183–5190.

242 H. Kim, K. Ryoul Park and C. Kim, *Opt. Express*, 2020, **28**, 1805–1816.

243 X. Shi, W. Xiao, Q. Fan, T. Zhou, W. Song, C. Zhang, Y. Zeng and W. Peng, *IEEE Sens. J.*, 2018, **18**, 9203–9206.

244 W. Li, Z. J. Coppens, L. V. Besteiro, W. Wang, A. O. Govorov and J. Valentine, *Nat. Commun.*, 2015, **6**, 8379.

245 M. Cotrufo, C. I. Osorio and A. F. Koenderink, *ACS Nano*, 2016, **10**, 3389–3397.

246 X.-T. Kong, L. Khosravi Khorashad, Z. Wang and A. O. Govorov, *Nano Lett.*, 2018, **18**, 2001–2008.

247 P. Spaeth, S. Adhikari, L. Le, T. Jollans, S. Pud, W. Albrecht, T. Bauer, M. Caldarola, L. Kuipers and M. Orrit, *Nano Lett.*, 2019, **19**, 8934–8940.

248 L. A. McCarthy, S. A. Hosseini Jebeli and S. Link, *J. Phys. Chem. C*, 2021, **125**, 4092–4101.

249 L. A. McCarthy, K. W. Smith, X. Lan, S. A. Hosseini Jebeli, L. Bursi, A. Alabastri, W.-S. Chang, P. Nordlander and S. Link, *Proc. Natl. Acad. Sci. U. S. A.*, 2020, **117**, 16143.

250 D. C. Hooper, A. G. Mark, C. Kuppe, J. T. Collins, P. Fischer and V. K. Valev, *Adv. Mater.*, 2017, **29**, 1605110.

251 M. Ren, E. Plum, J. Xu and N. I. Zheludev, *Nat. Commun.*, 2012, **3**, 833.

252 S. Chen, B. Reineke, G. Li, T. Zentgraf and S. Zhang, *Nano Lett.*, 2019, **19**, 6278–6283.

253 N. R. Famularo, L. Kang, Z. Li, T. Zhao, K. L. Knappenberger, C. D. Keating and D. H. Werner, *J. Chem. Phys.*, 2020, **153**, 154702.

254 S. P. Rodrigues, S. Lan, L. Kang, Y. Cui and W. Cai, *Adv. Mater.*, 2014, **26**, 6157–6162.

255 L. Ohnoutek, N. H. Cho, A. W. Allen Murphy, H. Kim, D. M. Răsădean, G. D. Pantoş, K. T. Nam and V. K. Valev, *Nano Lett.*, 2020, **20**, 5792–5798.

256 D. Kim, J. Yu, I. Hwang, S. Park, F. Demmerle, G. Boehm, M.-C. Amann, M. A. Belkin and J. Lee, *Nano Lett.*, 2020, **20**, 8032–8039.

257 W.-P. Guo, W.-Y. Liang, C.-W. Cheng, W.-L. Wu, Y.-T. Wang, Q. Sun, S. Zu, H. Misawa, P.-J. Cheng, S.-W. Chang, H. Ahn, M.-T. Lin and S. Gwo, *Nano Lett.*, 2020, **20**, 2857–2864.

258 F. Wang and H. Harutyunyan, *Adv. Opt. Mater.*, 2019, **7**, 1900744.

259 R. Narayanan and M. A. El-Sayed, *J. Phys. Chem. B*, 2005, **109**, 12663–12676.

260 R. J. White, R. Luque, V. L. Budarin, J. H. Clark and D. J. Macquarrie, *Chem. Soc. Rev.*, 2009, **38**, 481–494.

261 S. Shaw and J. D. White, *Chem. Rev.*, 2019, **119**, 9381–9426.

262 E. Pedrueza-Villalmanzo, F. Pineider and A. Dmitriev, *Nanophotonics*, 2020, **9**, 481–489.

263 C. Wattanakit, Y. B. S. Côme, V. Lapeyre, P. A. Bopp, M. Heim, S. Yadnum, S. Nokbin, C. Warakulwit, J. Limtrakul and A. Kuhn, *Nat. Commun.*, 2014, **5**, 3325.

264 T. Yutthalekha, C. Wattanakit, V. Lapeyre, S. Nokbin, C. Warakulwit, J. Limtrakul and A. Kuhn, *Nat. Commun.*, 2016, **7**, 12678.

265 S. Assavapanumat, M. Ketkaew, A. Kuhn and C. Wattanakit, *J. Am. Chem. Soc.*, 2019, **141**, 18870–18876.

266 L. Ma, Y. Cao, Y. Duan, L. Han and S. Che, *Angew. Chem., Int. Ed.*, 2017, **56**, 8657–8662.

267 H. Liu, Z. Li, Y. Yan, J. Zhao and Y. Wang, *Nanoscale*, 2019, **11**, 21990–21998.

268 X. Wei, J. Liu, G.-J. Xia, J. Deng, P. Sun, J. J. Chruma, W. Wu, C. Yang, Y.-G. Wang and Z. Huang, *Nat. Chem.*, 2020, **12**, 551–559.

269 H. Niinomi, T. Sugiyama, M. Tagawa, K. Murayama, S. Harada and T. Ujihara, *CrystEngComm*, 2016, **18**, 7441–7448.

270 A.-C. Cheng, H. Niinomi, T. Omatsu, S. Ishida, K. Sasaki and T. Sugiyama, *J. Phys. Chem. Lett.*, 2020, **11**, 4422–4426.

271 H. Niinomi, T. Sugiyama, A.-C. Cheng, M. Tagawa, T. Ujihara, H. Y. Yoshikawa, R. Kawamura, J. Nozawa,

J. T. Okada and S. Uda, *J. Phys. Chem. C*, 2021, **125**, 6209–6221.

272 C. Hao, L. Xu, W. Ma, X. Wu, L. Wang, H. Kuang and C. Xu, *Adv. Funct. Mater.*, 2015, **25**, 5816–5822.

273 T. Liu, L. V. Besteiro, T. Liedl, M. A. Correa-Duarte, Z. Wang and A. O. Govorov, *Nano Lett.*, 2019, **19**, 1395–1407.

274 W. Wang, L. V. Besteiro, T. Liu, C. Wu, J. Sun, P. Yu, L. Chang, Z. Wang and A. O. Govorov, *ACS Photonics*, 2019, **6**, 3241–3252.

275 L. K. Khorashad, L. V. Besteiro, M. A. Correa-Duarte, S. Burger, Z. M. Wang and A. O. Govorov, *J. Am. Chem. Soc.*, 2020, **142**, 4193–4205.

276 J. A. Hutchison, T. Schwartz, C. Genet, E. Devaux and T. W. Ebbesen, *Angew. Chem., Int. Ed.*, 2012, **51**, 1592–1596.

277 A. Thomas, J. George, A. Shalabney, M. Dryzhakov, S. J. Varma, J. Moran, T. Chervy, X. Zhong, E. Devaux, C. Genet, J. A. Hutchison and T. W. Ebbesen, *Angew. Chem.*, 2016, **128**, 11634–11638.

278 A. Thomas, L. Lethuillier-Karl, K. Nagarajan, R. M. Vergauwe, J. George, T. Chervy, A. Shalabney, E. Devaux, C. Genet and J. Moran, *Science*, 2019, **363**, 615–619.

279 Y. Pang, A. Thomas, K. Nagarajan, R. M. A. Vergauwe, K. Joseph, B. Patrahau, K. Wang, C. Genet and T. W. Ebbesen, *Angew. Chem., Int. Ed.*, 2020, **59**, 10436–10440.

280 J. Garcia-Vidal Francisco, C. Ciuti and T. W. Ebbesen, *Science*, 2021, **373**, eabd0336.

281 M. Hertzog, M. Wang, J. Mony and K. Börjesson, *Chem. Soc. Rev.*, 2019, **48**, 937–961.

282 H. Hübener, U. De Giovannini, C. Schäfer, J. Andberger, M. Ruggenthaler, J. Faist and A. Rubio, *Nat. Mater.*, 2021, **20**, 438–442.

283 M. L. Solomon, A. A. E. Saleh, L. V. Poulikakos, J. M. Abendroth, L. F. Tadesse and J. A. Dionne, *Acc. Chem. Res.*, 2020, **53**, 588–598.

284 A. O. Govorov, Z. Fan, P. Hernandez, J. M. Slocik and R. R. Naik, *Nano Lett.*, 2010, **10**, 1374–1382.

285 Y. Chen, C. Zhao, Y. Zhang and C. Qiu, *Nano Lett.*, 2020, **20**, 8696–8703.

286 J. Lasa-Alonso, D. R. Abujetas, Á. Nodar, J. A. Dionne, J. J. Sáenz, G. Molina-Terriza, J. Aizpurua and A. García-Etxarri, *ACS Photonics*, 2020, **7**, 2978–2986.

287 T. V. Raziman, R. H. Godiksen, M. A. Müller and A. G. Curto, *ACS Photonics*, 2019, **6**, 2583–2589.

288 E. Mohammadi, A. Tittl, K. L. Tsakmakidis, T. V. Raziman and A. G. Curto, *ACS Photonics*, 2021, **8**, 1754–1762.

289 Y. Wang, Z. Wang, Q. Wang, S. Zhou, Q. Han, W. Gao, K. Ren, J. Qi and J. Dong, *J. Phys. Chem. C*, 2019, **123**, 24754–24762.

290 L. Xu, Z. Xu, W. Ma, L. Liu, L. Wang, H. Kuang and C. Xu, *J. Mater. Chem. B*, 2013, **1**, 4478–4483.

291 L. D. Barron, M. P. Bogaard and A. D. Buckingham, *J. Am. Chem. Soc.*, 1973, **95**, 603–605.

292 B. Bosnich, M. Moskovits and G. A. Ozin, *J. Am. Chem. Soc.*, 1972, **94**, 4750–4751.

293 S. Efrima, *Chem. Phys. Lett.*, 1983, **102**, 79–82.

294 L. Hecht and L. D. Barron, *Chem. Phys. Lett.*, 1994, **225**, 525–530.

295 S. Abdali and E. W. Blanch, *Chem. Soc. Rev.*, 2008, **37**, 980–992.

296 C. Johannessen, P. C. White and S. Abdali, *J. Phys. Chem. A*, 2007, **111**, 7771–7776.

297 T. A. Keiderling, *Chem. Rev.*, 2020, **120**, 3381–3419.

298 R. Acevedo, R. Lombardini, N. J. Halas and B. R. Johnson, *J. Phys. Chem. A*, 2009, **113**, 13173–13183.

299 D. V. Chulhai and L. Jensen, *J. Phys. Chem. A*, 2014, **118**, 9069–9079.

300 L. Hu, F. Xi, L. Qv and Y. Fang, *ACS Omega*, 2018, **3**, 1170–1177.

301 M. Sun, Z. Zhang, P. Wang, Q. Li, F. Ma and H. Xu, *Light: Sci. Appl.*, 2013, **2**, e112.

302 X. Ren, W. Lin, Y. Fang, F. Ma and J. Wang, *RSC Adv.*, 2017, **7**, 34376–34381.

303 M. Das, D. Gangopadhyay, J. Šebestík, L. Habartová, P. Michal, J. Kapitán and P. Bouř, *Chem. Commun.*, 2021, **57**, 6388–6391.

304 S. O. Pour, S. E. J. Bell and E. W. Blanch, *Chem. Commun.*, 2011, **47**, 4754–4756.

305 S. Ostovar pour, L. Rocks, K. Faulds, D. Graham, V. Parchaňský, P. Bouř and E. W. Blanch, *Nat. Chem.*, 2015, **7**, 591–596.

306 S. Abdali, C. Johannessen, J. Nygaard and T. Nørbygaard, *J. Phys.: Condens. Matter*, 2007, **19**, 285205.

307 X. Sun, H. Kong, Q. Zhou, S. Tsunega, X. Liu, H. Yang and R.-H. Jin, *Anal. Chem.*, 2020, **92**, 8015–8020.

308 Y. Kalachyova, O. Guselnikova, R. Elashnikov, I. Panov, J. Žádný, V. Církva, J. Storch, J. Sykora, K. Zaruba, V. Švorčík and O. Lyutakov, *ACS Appl. Mater. Interfaces*, 2019, **11**, 1555–1562.

309 Z. Liu, J. Ai, P. Kumar, E. You, X. Zhou, X. Liu, Z. Tian, P. Bouř, Y. Duan, L. Han, N. A. Kotov, S. Ding and S. Che, *Angew. Chem., Int. Ed.*, 2020, **59**, 15226–15231.

310 R. Tullius, A. S. Karimullah, M. Rodier, B. Fitzpatrick, N. Gadegaard, L. D. Barron, V. M. Rotello, G. Cooke, A. Lapthorn and M. Kadodwala, *J. Am. Chem. Soc.*, 2015, **137**, 8380–8383.

311 Y. Zhao, A. N. Askarpour, L. Sun, J. Shi, X. Li and A. Alù, *Nat. Commun.*, 2017, **8**, 14180.

312 L. Yang, C.-S. Kwan, L. Zhang, X. Li, Y. Han, K. C.-F. Leung, Y. Yang and Z. Huang, *Adv. Funct. Mater.*, 2019, **29**, 1807307.

313 A. S. Karimullah, C. Jack, R. Tullius, V. M. Rotello, G. Cooke, N. Gadegaard, L. D. Barron and M. Kadodwala, *Adv. Mater.*, 2015, **27**, 5610–5616.

314 H.-H. Jeong, A. G. Mark, M. Alarcón-Correa, I. Kim, P. Oswald, T.-C. Lee and P. Fischer, *Nat. Commun.*, 2016, **7**, 11331.

315 M. Rodier, C. Keijzer, J. Milner, A. S. Karimullah, L. D. Barron, N. Gadegaard, A. J. Lapthorn and M. Kadodwala, *J. Phys. Chem. Lett.*, 2019, **10**, 6105–6111.

316 W.-F. Lau, L. Yang, F. Bai and Z. Huang, *Small*, 2016, **12**, 6698–6702.

317 M. Matuschek, D. P. Singh, H.-H. Jeong, M. Nesterov, T. Weiss, P. Fischer, F. Neubrech and N. Liu, *Small*, 2018, **14**, 1702990.

318 X. Duan, S. Kamin, F. Sterl, H. Giessen and N. Liu, *Nano Lett.*, 2016, **16**, 1462–1466.

319 Y. Zhao, L. Xu, W. Ma, L. Wang, H. Kuang, C. Xu and N. A. Kotov, *Nano Lett.*, 2014, **14**, 3908–3913.

320 W. Yan, L. Xu, W. Ma, L. Liu, L. Wang, H. Kuang and C. Xu, *Small*, 2014, **10**, 4293–4297.

321 C. Hao, L. Xu, M. Sun, W. Ma, H. Kuang and C. Xu, *Adv. Funct. Mater.*, 2018, **28**, 1802372.

322 D. Meng, W. Ma, X. Wu, C. Xu and H. Kuang, *Small*, 2020, **16**, 2000003.

323 L. Xu, Y. Gao, H. Kuang, L. M. Liz-Marzán and C. Xu, *Angew. Chem., Int. Ed.*, 2018, **57**, 10544–10548.

324 S. Li, L. Xu, W. Ma, X. Wu, M. Sun, H. Kuang, L. Wang, N. A. Kotov and C. Xu, *J. Am. Chem. Soc.*, 2016, **138**, 306–312.

325 T. Funck, F. Nicoli, A. Kuzyk and T. Liedl, *Angew. Chem., Int. Ed.*, 2018, **57**, 13495–13498.

326 T. Funck, T. Liedl and W. Bae, *Appl. Sci.*, 2019, **9**, 3006.

327 Z. Liu, J. Dong, J. Pan, C. Zhou, C. Fan and Q. Wang, *Chem. Res. Chin. Univ.*, 2021, **37**, 914–918.

328 Y. Huang, M.-K. Nguyen, A. K. Natarajan, V. H. Nguyen and A. Kuzyk, *ACS Appl. Mater. Interfaces*, 2018, **10**, 44221–44225.

329 J. Dong, M. Wang, Y. Zhou, C. Zhou and Q. Wang, *Angew. Chem., Int. Ed.*, 2020, **59**, 15038–15042.

330 S. V. Boriskina, T. A. Cooper, L. Zeng, G. Ni, J. K. Tong, Y. Tsurimaki, Y. Huang, L. Meroueh, G. Mahan and G. Chen, *Adv. Opt. Photonics*, 2017, **9**, 775–827.

331 L. Jauffred, A. Samadi, H. Klingberg, P. M. Bendix and L. B. Oddershede, *Chem. Rev.*, 2019, **119**, 8087–8130.

332 J. B. Vines, J.-H. Yoon, N.-E. Ryu, D.-J. Lim and H. Park, *Front. Chem.*, 2019, **7**, 167.

333 B. Wild, L. Cao, Y. Sun, B. P. Khanal, E. R. Zubarev, S. K. Gray, N. F. Scherer and M. Pelton, *ACS Nano*, 2012, **6**, 472–482.

334 M. I. Stockman, *Phys. Rev. Lett.*, 2011, **106**, 156802.

335 M. Decker and I. Staude, *J. Opt.*, 2016, **18**, 103001.